

TransKD: Transformer Knowledge Distillation for Efficient Semantic Segmentation

Ruiping Liu, Kailun Yang*, Alina Roitberg, Jiaming Zhang, Kunyu Peng, Huayao Liu, and Rainer Stiefelhagen

Abstract—Large pre-trained transformers are on top of contemporary semantic segmentation benchmarks, but come with high computational cost and a lengthy training. To lift this constraint, we look at efficient semantic segmentation from a perspective of comprehensive knowledge distillation and consider to bridge the gap between multi-source knowledge extractions and transformer-specific patch embeddings. We put forward the *Transformer-based Knowledge Distillation (TransKD)* framework which learns compact student transformers by distilling both feature maps and patch embeddings of large teacher transformers, bypassing the long pre-training process and reducing the FLOPs by $>85.0\%$. Specifically, we propose two fundamental and two optimization modules: (1) *Cross Selective Fusion (CSF)* enables knowledge transfer between cross-stage features via channel attention and feature map distillation within hierarchical transformers; (2) *Patch Embedding Alignment (PEA)* performs dimensional transformation within the patchifying process to facilitate the patch embedding distillation; (3) *Global-Local Context Mixer (GL-Mixer)* extracts both global and local information of a representative embedding; (4) *Embedding Assistant (EA)* acts as an embedding method to seamlessly bridge teacher and student models with the teacher's number of channels. Experiments on Cityscapes, ACDC, and NYUv2 datasets show that TransKD outperforms state-of-the-art distillation frameworks and rivals the time-consuming pre-training method. Code is available at [TransKD](#).

Index Terms—Knowledge Distillation, Semantic Segmentation, Scene Parsing, Vision Transformer, Scene Understanding.

1 INTRODUCTION

SEMANTIC segmentation assigns category labels at a pixel-level (see examples in Fig. 1) and is a crucial tool in a wide range of applications, such as robot grasping [1], [2], autonomous driving [3], [4], and navigation assistance for people with visual impairments [5], [6]. Driven by the success of deep learning, semantic segmentation enables fine-grained scene understanding with impressive accuracies [7], [8], but relatively little consideration has been given to the computational constraints of real-life systems, such as inference and training speed or memory footprint.

While Convolutional Neural Networks (CNNs) have been the visual recognition frontrunners for almost a decade, they face problems capturing large-scale interactions due to their focus on local neighbourhood operations and limited receptive fields. Vision transformers [7], [8], [9] overcome this challenge through the concept of self-attention [10], which learns to intensify or weaken portions of input at a global scale. This excellent quality of modelling long-range dependencies has lead to transformers being on top of virtually all semantic segmentation benchmarks [7], [8], [9]. Unfortunately, transformers are usually very large and require a long training process due to the lack of inductive bias compared to CNNs [9]. Thus, vision transformers often show less satisfactory performance on smaller task-specific datasets, and time-consuming pre-training process on a massive dataset is entailed [7], [9], e.g., 100 epochs on ImageNet [11] across multiple devices. The high computational and training costs constitute a

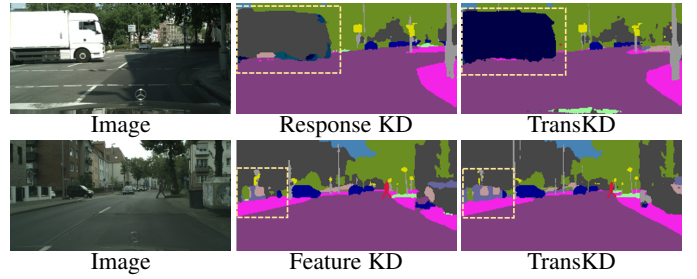


Fig. 1: Hard examples for semantic segmentation with knowledge distillation methods. We exhibit the segmentation results of current knowledge distillation frameworks as counterparts, which extract the knowledge from responses [14] and the relationship among feature maps [15], respectively. Our framework, TransKD, enables the model to predict the *truck* and *fence* more precisely by exploring the knowledge from both feature maps and patch embeddings.

significant bottleneck for real applications, where cumbersome models cannot be deployed on mobile devices, whereas smaller models suffer from inaccurate predictions [12], [13].

A popular way to reduce the computational cost is *knowledge distillation* [16] which offers a mechanism for an effective knowledge transfer between a large teacher model and a smaller student network and has been widely studied for deep CNNs [12], [14], [15]. Gou *et al.* [17] distinguish three types of knowledge to be distilled (see Fig. 2 a-c): response-based knowledge [12], [14], [16], feature-based knowledge [12], [18], [19], and relation-based knowledge [15], [20], [21]. The response-based and feature-based knowledge distillation utilize the output of a single specific layer of the teacher model (the last or the intermediate layer respectively), whereas the relation-based knowledge distillation tracks

• R. Liu, K. Yang, J. Zhang, A. Roitberg, K. Peng, and R. Stiefelhagen are with Institute for Anthropomatics and Robotics, Karlsruhe Institute of Technology, 76131 Karlsruhe, Germany. (E-Mail: liuruipinglena@hotmail.com, kailun.yang@kit.edu, alina.roitberg@kit.edu, jiaming.zhang@kit.edu, kunyu.peng@kit.edu, rainer.stiefelhagen@kit.edu.)
 • H. Liu is with NIO, Shanghai 201804, China. (E-Mail: huayao.liu@outlook.com.)
 • * corresponding author.

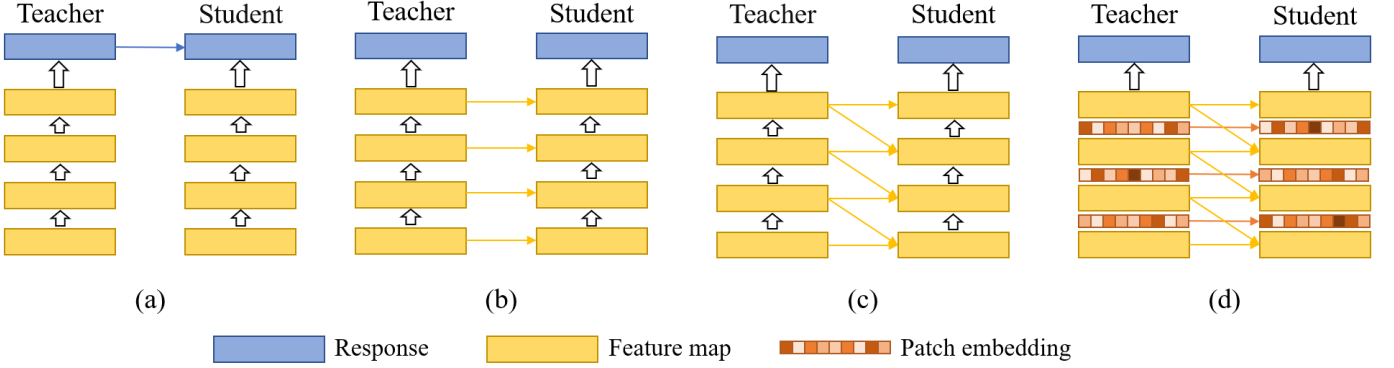


Fig. 2: (a)-(c) Knowledge distillation in computer vision is split into three categories according to Gou *et al.* [17]: response-based knowledge distillation, feature-based knowledge distillation, and relation-based knowledge distillation. (d) Our knowledge distillation framework extracts the relation-based knowledge of feature maps and transformer-specific patch embedding knowledge at each stage.

the relationship between multiple layers simultaneously. These paradigms are mainly designed with the CNN-to-CNN transfer in mind [12], [14], [15] and do not sufficiently cover knowledge distillation from transformer-specific intermediate blocks, such as the patch embeddings, resulting in less satisfactory segmentation maps, as illustrated in Fig. 1.

In the light of high computational costs and long pre-training of visual transformers, we pose the following question: is it possible to build lightweight models by taking advantage of knowledge sources present in the intermediate representations of large-scale transformers? To reach our goal of efficient semantic segmentation, we propose *Transformer-based Knowledge Distillation (TransKD)*, the first framework for distilling knowledge from large-scale semantic segmentation transformers. We focus on a comprehensive distillation from different knowledge sources within the transformer-specific building blocks (our key idea is presented in Fig. 2 d). Specifically, TransKD distills the information from both (1) *feature maps* and (2) the transformer-specific *patch embeddings*. Explicitly contemplating the patch embeddings is important as they carry substantial information within the transformers [9], [22], [23], which differs from the one contained in the feature maps not only through the distinct shape and dimensionality, but also in the inherent knowledge acquired through the patchifying process enabling sequence-to-sequence learning. We believe that extracting information not only from the feature maps but also from the transformer-specific patch embeddings harvests both, spatial and sequential relationships and is therefore important to maximize the potential of transformer-to-transformer knowledge distillation.

Specifically, we design two fundamental and two optimization modules within the TransKD framework. (1) For feature map distillation, we build a relation-based scheme atop Knowledge Review [15] and introduce the *Cross Selective Fusion (CSF)* module to merge cross-stage feature maps via channel attention and construct the feature map distillation streams within hierarchical transformers. (2) For patch embedding distillation, we introduce a fundamental *Patch Embedding Alignment (PEA)* module to perform dimensional transformation of patch embeddings along the channel dimension to facilitate multi-stage patch embedding distillation streams. (3) As known to the field, both neighbouring and long-range relationships are vital for semantic segmentation [22], [24], our *Global-Local Context Mixer (GL-Mixer)* extracts both global and local information of a representative

embedding for distillation. (4) Furthermore, considering that the large gap between the student's and the teacher's size negatively impacts the knowledge distillation results [25], [26], we present an *Embedding Assistant (EA)* module, which acts an embedder with teacher's number of channels. EA helps to build a pseudo teacher assistant model by combining the student's transformer blocks and seamlessly bridge teacher and student models.

We demonstrate the benefits of our approach for real-world mobile applications on three benchmarks: a general street scene dataset (Cityscapes [27]), an adverse street scene dataset (ACDC [28]), and an indoor understanding dataset (NYUv2 [29]). Comprehensive experiments showcase that our framework outperforms state-of-the-art knowledge distillation counterparts by a large gap. Compared to the cumbersome teacher model, TransKD reduces the floating-point operations (FLOPs) by >85.0%, while keeping competitive accuracy. By unifying patch embedding and feature map distillation, TransKD robustifies the segmentation of hard examples where previous paradigms struggle, as shown in Fig. 1. Benchmarked against the feature-map-only method Knowledge Review [15], TransKD enhances the distillation performance by >5.0% in mean Intersection over Union (mIoU). On Cityscapes, TransKD improves the mIoU of the non-pretrained SegFormer B0 [22] by 13.12%. We also consider various dense prediction and semantic segmentation transformers [22], [30], [31] and verify that TransKD consistently boosts the accuracy of compact segmenters. Lastly, TransKD rivals the performance of the time-consuming pre-trained method. Our best model achieves 75.74% in mIoU with only 3.72M parameters.

At a glance, this work delivers the following contributions:

- We are the first to propose a transformer-to-transformer knowledge distillation framework in semantic segmentation and to utilize the transformer-specific patch embedding as one of the knowledge sources.
- We provide a new perspective on distilling knowledge from transformer-specific patch embeddings. Our TransKD framework unifies feature map- and patch embedding distillation.
- To this intent, we design two fundamental modules, *Cross Selective Fusion (CSF)* and *Patch Embedding Alignment (PEA)*, and two optimization modules, *Global-Local Context Mixer (GL-Mixer)* and *Embedding Assistant (EA)*.
- In-depth experiments validate the advantages of TransKD on Cityscapes, ACDC, and NYUv2 datasets with obvious improvements over existing knowledge distillation methods.

2 RELATED WORK

2.1 From Accurate to Efficient Semantic Segmentation

Semantic segmentation has witnessed tremendous progress since Fully Convolutional Networks (FCNs) [32] first looked at the pixel classification problem from an end-to-end perspective. Many subsequent networks followed this scheme, often raising its accuracy through encoder-decoder architectures [33] or aggregation of multi-scale context [24], [34], [35], [36], [37], [38]. An important cluster of methods leverages non-local self-attention [10], [39] to capture long-range contextual dependencies and encourage global reasoning [40], [41], [42], [43], [44]. Other main strategies for improving the segmentation outcomes include refining contextual priors [45], [46], [47] and exploiting boundary cues [48], [49], [50]. Recent success of vision transformers [9], [51], [52] lead to the development of multiple transformer-based architectures for semantic segmentation [7], [8], [53] which have since then become state-of-the-art on virtually all mainstream benchmarks [27], [28], [29], thanks to their ability to gather global dependencies from early layers via token mixing modules such as self-attention [10] or MLP-like blocks [54], [55]. Inspired by the detection transformer [56], researchers have also explored universal semantic- and panoptic segmentation through mask classification [57], [58], [59]. However, computational cost and lengthy training process remain a weak spot of the accuracy-driven transformer research.

On the other hand, multiple works explicitly address efficient semantic segmentation, aiming to strike a good balance between speed and accuracy. This line of research compactifies the architectures through techniques such as early downsampling [60], filter factorization [3], [13], multi-branch architecture [61], [62], [63], [64], and ladder-style upsampling [65], [66]. Lightweight classification backbones such as MobileNets [67] and ShuffleNets [68] have also been considered to speed-up image segmentation. SFNet [69] learns semantic flow between adjacent-level feature maps for efficiently broadcasting high-level features to high-resolution ones. SegBlocks [70] dynamically modulate the processing resolution of image regions, whereas TopFormer [71] uses tokens of various scales to enhance the representation in a SwiftNet [65]-like manner. Moreover, SegFormer [22] introduces a lightweight and efficient semantic segmentation framework, which unifies the backbone output feature maps with a simple MLP decoder. Both FAN [72] and iFormer [73] deploy parallel operators in token mixing blocks to strengthen the modeling of discriminative information. Unlike all these works, we look at resource-efficient segmentation transformers from a new perspective of comprehensive knowledge distillation and introduce a framework for simultaneously extracting knowledge from different blocks of large-scale vision transformers and re-using it for compact and fast student transformers.

2.2 Vision Transformer for Dense Prediction

Transformer architecture has become the de-facto standard in Natural Language Processing (NLP) mostly due to the effectiveness of stacked self-attention and its ability to capture long-range relationships within the data. The success of self-attention-based models has also spread within the field of visual recognition, starting with the introduction of the Vision Transformer (ViT) [9] – the first transformer delivering strong results on ImageNet [11]. Subsequent developments include DeiT [51], which utilizes token-based distillation to mimic a ViT model in a data-efficient manner and Dynamic ViT [74], which conducts distillation between the

original ViT and their efficient dynamic transformer with token sparsification. T2T-ViT [75] further introduces a progressive tokenization scheme, which recursively assembles neighboring tokens to model local structure and reduce the tokens length. Swin-T [76] and PVT [23], [30] are hierarchical transformer architectures with multi-scale feature maps, which have become standard backbones for various dense prediction tasks such as object detection and semantic segmentation. Twins [77] and UniFormer [78] leverage conditional positionsl encoding [79] to unleash the transformer’s ability to process arbitrary input size and improve dense recognition. Following this idea, a variety of dense prediction vision transformers [80], [81], [82], [83], [84], [85], [86] have emerged. The recently introduced vision transformer adapter [87] incorporates image priors into ViT to supplement local continuity cues and multi-scale features, which makes the vanilla ViT better suitable for dense predictions.

At the same time, multiple lightweight vision transformers [88], [89], [90], [91] have emerged. For example, LeViT [88] is a hybrid model re-using ResNet stages within the transformer architecture while MobileViT [92] leverages MoibleNetV2 blocks [67] along the downsampling path and Mobile-Former [93] establishes a dual-stream architecture by bridging MobileNet and its transformer branch. EfficientViT [89] substitutes the Softmax-based attention with linear attention and encourages the powerful local features via depthwise convolution. Unfortunately, recent studies [92] suggest that MobileViT and other ViT-based models are still not efficient enough for real-time processing on mobile devices. In this work, we develop a knowledge distillation framework based on vision transformers, which consistently improves the performance of compact dense prediction and semantic segmentation transformers [22], [30], [31], leading to a much better trade-off of accuracy, computational cost, and pre-training requirements.

2.3 Knowledge Distillation for Semantic Segmentation

Hinton *et al.* [16] introduced the concept of Knowledge Distillation (KD), which learns to transfer the knowledge from a large-scale model to a more compact one. These two models behave like a teacher and a student and this paradigm is widely used in computer vision [17], [94]. In this work, our goal is to study and design a KD framework specifically for semantic segmentation with transformer-based models.

KD approaches have been grouped [17], [94] into three categories based on the form of knowledge: response-based KD [12], [14], [18], [95], [95], [96], [97], feature-based KD [14], [18], [19], [98], [99], [100], [101], [102], [103], [104], and relation-based KD [15], [20], [21], [105]. Liu *et al.* [12] first introduced the idea of structured knowledge distillation, where adversarial learning is used to align the segmentation map produced by the compact student network with the one of the cumbersome teacher network. Knowledge Review (KR) [15] for the first time proposed to distill knowledge using cross-stage connection paths. Double Similarity Distillation (DSD) [20] transfers both detailed spatial dependencies and global category correlations. Unlike previous works mostly devoted to the distillation of spatial-wise knowledge, some recent works focus on the distillation of channel-wise distribution. Intra-class Feature Variation Distillation (IFVD) [18] passes on the variations of intra-class representations between the networks. Channel Distillation (CD) [14] focuses on the soft distributions of channels and pays attention to the most salient parts of the channel-wise maps. Inter-channel Correlation Knowledge

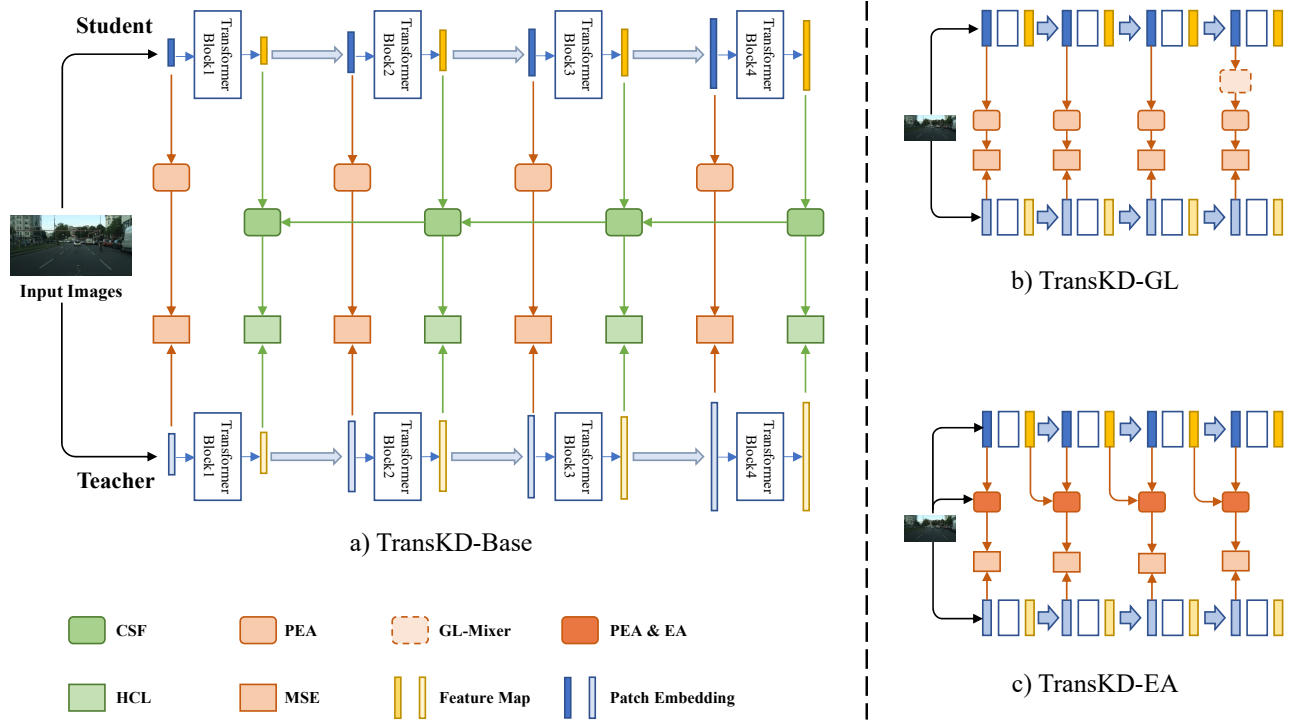


Fig. 3: Our knowledge distillation framework TransKD. It is divided into two parts: knowledge distillation of patch embeddings (red arrows and rectangles) and feature maps (green arrows and rectangles). The loss function consists of two distillation terms (HCL and MSE) and a cross-entropy term. (a) TransKD-Base is the basic version of TransKD, constructed with two fundamental modules, CSF and PEA. (b) TransKD-GL and (c) TransKD-EA are two optimized versions of TransKD.

Distillation (ICKD) [99] aligns the diversity and homology of the student model’s feature space with that of the teacher network.

Additionally, knowledge adaptation is addressed in [106] by optimizing affinity distillation. Adaptive Perspective Distillation (APD) [107] mines detailed contextual cues from each training sample, whereas [108] follows a hierarchical distillation approach and enables a one-to-all spatial matching. Furthermore, data distillation [109] is explored in [4] for omnidirectional semantic segmentation, whereas [110] proposes uncertainty-aware contrastive distillation to alleviate catastrophic forgetting in incremental learning. All of these works are dedicated to CNN-to-CNN or CNN-to-transformer knowledge distillation. In contrast, our proposed TransKD model explores this concept in a novel transformer-to-transformer fashion, by explicitly considering multi-source knowledge within the transformer architecture and taking transformer-specific patch embeddings into account.

3 PROPOSED FRAMEWORK: TRANSKD

3.1 Overview

At the heart of this work is the transformer-to-transformer knowledge transfer for efficient semantic segmentation. To strike a better balance between accuracy, computational costs, and the required amount of pre-training, we for the first time look at semantic segmentation through the lens of *multi-source knowledge distillation* within visual transformers. While transformer-to-transformer knowledge distillation is explored in natural language processing [111], [112], [113], it has been rather overlooked in semantic segmentation and vision transformers in general, where most of the models still center around CNN-based knowledge

distillation. Adopting such methods to suit visual transformers is not trivial due to diverging architecture-specific building blocks arising, *e.g.*, from the patchifying process.

Existing semantic segmentation transformers generally follow either an isotropic structure [7], [72], [87] or a four-stage hierarchical structure [22], [23], [30], [31], [83]. Since the latter one is better at modelling multi-scale long-range information [23], [76], it is more versatile in dense prediction tasks such as pixel-wise semantic segmentation. Thereby, in this work, knowledge distillation is carried out on four-stage transformers (see Fig. 3).

The first step of the general visual transformer pipeline is to “patchify” the input \mathbf{I} (an image or a feature map):

$$\mathbf{E} = \text{PatchEmbed}(\mathbf{I}). \quad (1)$$

This “patchification” is the key ingredient of vision transformers as it allows us to cast vision-based tasks as sequence-to-sequence problems for which this type of models was initially built [10]. The patch embedding module splits the input images or feature maps $\mathbf{I} \in \mathbb{R}^{C \times H \times W}$ into patches and transforms these patches (mostly via a convolution operation) into a representative patch embedding $\mathbf{E} \in \mathbb{R}^{N \times C'}$, where N is the number of patches and C' the number of the channels. As often highlighted in previous research, the resulting patch embeddings convey important information about long-range sequential relationships [7], [82], location priors [7], [9], [72], and local continuity cues [22], [30], [83].

Next, the patch embeddings are passed to a stack of transformer encoding layers consisting of a multi-head self-attention and a position-wise fully connected feed-forward network [9], [10]. The outputs of these layers are then reshaped into a feature

map \mathbf{F} :

$$\mathbf{F} = \text{TransformerEncode}(\mathbf{E}), \quad (2)$$

where the feature map $\mathbf{F} \in \mathbb{R}^{C' \times H' \times W'}$ marks the output of the current transformer stage and therefore the input to the next layer. A positive consequence of self-attention exploring all the patch tokens with no restriction to a certain receptive field is that the *global* context also being covered in the resulting feature map. Distilling knowledge from both, feature maps and patch embeddings, allows us to track complementary information within the transformer, such as spatial and sequential relationships.

Motivated by this, we propose *Transformer-based Knowledge Distillation (TransKD)* – a novel transformer-to-transformer knowledge distillation framework with the overall goal of building small yet accurate semantic segmentation transformers less reliant on time-consuming pre-training. TransKD centers around two types of knowledge transfer: (1) patch embedding distillation and (2) feature map distillation. The *patch embedding distillation* is performed at each of the four transformer stages while the feature map distillation leverages the relation-based knowledge distillation to gather information from within-stage and cross-stage feature maps. An overview of this core pipeline is depicted in Fig. 3(a).

The distillation losses obtained from each stage are added to the original cross-entropy loss L_{CE} during training. The overall KD loss then becomes:

$$L = L_{CE} + \sum_{m=1}^M \alpha_m L_{embd}^m + \sum_{m=1}^M \beta_m L_{f'm}^m, \quad (3)$$

where L_{embd}^m and $L_{f'm}^m$ refer to the patch embedding loss and the feature map loss between the m -th stage of the teacher and the student. As mentioned before, we explore the typical four-stage transformer in this work, *i.e.*, $M = 4$ in our case. α_m and β_m are the m -th elements of α and β , which control the weights of the patch embedding loss and the feature map loss at each stage, respectively. α and β are set as $[0.1, 0.1, 0.5, 1]$ and $[1, 1, 1, 1]$. In the following method descriptions, matrices with superscripts *in* and *out* refer to inputs and outputs of the proposed modules, and matrices with the superscript *mid* refer to processed matrices within the modules.

In Sec. 3.2, we present the design of our patch embedding distillation scheme, and in Sec. 3.3 we elaborate our feature map distillation method. Finally, in Sec. 3.4, we describe the configurations of different variants of the TransKD framework.

3.2 Patch Embedding Distillation

To maximize the potential of transformer-to-transformer knowledge distillation, we consider that transformer-specific patch embeddings should be fully exploited. The patch embedding channels of the student and the teacher models are different and a dimensionality transformation is an essential prerequisite step for patch embedding distillation at different network depths. To meet this requirement, we propose the *Patch Embedding Alignment (PEA)* module, which acts as a fundamental module for the channel dimension transformation. Additionally, we design the *Global-Local Context Mixer (GL-Mixer)* and the *Embedding Assistant (EA)* to optimize patch embedding distillation.

Patch embedding alignment. We conduct the Patch Embedding Alignment (PEA) through a linear projection for dimensionality transformation, after which the MSE loss between the student and teacher patch embeddings is calculated, as depicted in Eq. (4):

$$L_{embd}^m = \text{MSE}(\mathbf{E}_m^S \mathbf{W}_e, \mathbf{E}_m^T), \quad (4)$$

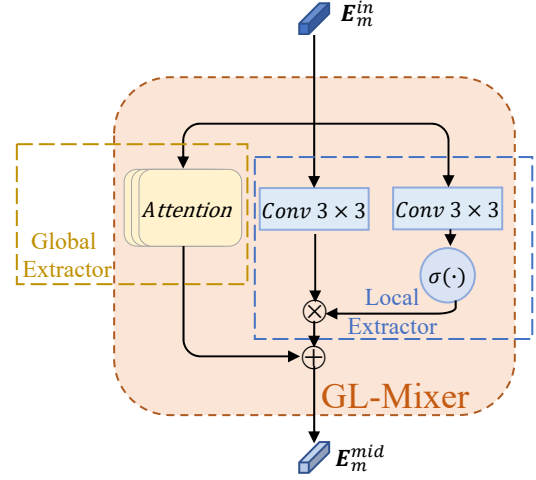


Fig. 4: Two-branch architecture of Global-Local Context Mixer (GL-Mixer) in Fig. 3(b). The global context of an embedding is extracted by multi-head attention mechanisms, whereas the local features are extracted by convolution operations.

where \mathbf{E}_m^S and \mathbf{E}_m^T are the patch embeddings at the m -th student and teacher stages. A learnable matrix \mathbf{W}_e is applied to counter the dimensionality mismatch. PEA bridges the teacher and student transformers and facilitates the multi-stage patch embedding streams, while only adding marginal computational complexity.

Global-local context mixer. Patch embeddings deliver heterogeneous patterns [9], [22]. Therefore, the global context cues and the fine-grained local features, which are essential for semantic segmentation, cannot be fully distilled by using linear projection alone. With this in mind, we propose the *Global-Local Context Mixer (GL-Mixer)*, which follows a two-branch design, where the branches are individually specialized on global or local information. The global context is extracted via multi-head attention (left branch in Fig. 4) and the local information is extracted via convolution operations (right branch in Fig. 4). Inspired by the Gated Linear Unit (GLU) function [114], [115], a sigmoid function $\sigma(\cdot)$ is used to control the information flow. Given an input patch embedding \mathbf{E}_m^{in} , the two-branch processing of global and local cues inside the GL-Mixer is formalized in Eq. (5):

$$\begin{aligned} \text{GL-Mixer}(\mathbf{E}_m^{\text{in}}) = & \text{MultiHeadAttn}(\mathbf{E}_m^{\text{in}}) \\ & + (\mathbf{E}_m^{\text{in}} * \mathbf{W} + \mathbf{a}) \otimes (\sigma(\mathbf{E}_m^{\text{in}} * \mathbf{V} + \mathbf{b})), \end{aligned} \quad (5)$$

where \mathbf{W} , \mathbf{V} , \mathbf{a} , and \mathbf{b} refer to learnable parameters for the convolutional operations. As shown in Fig. 4, the convolution operations are implemented via 3×3 convolutions and the entire GL-Mixer is lightweight. This way, given a representative patch embedding within a dense prediction transformer, both the semantically-rich global context and the detail-rich local features can be harvested for distillation.

Embedding assistant. Knowledge distillation runs into problems when the size gap between student and teacher is significant [25], [26]. If the teacher becomes very complex, the student eventually lacks the sufficient capacity or mechanics to mimic its behavior despite receiving multi-stage hints. Mirzadeh *et al.* [25] introduce a Teacher Assistant (TA) of an intermediate size to bridge the size gap. TA acts as a mediator between the teacher and the student: it is distilled from the teacher model and then passes the knowledge to the student. TA follows the same structure as the student and the

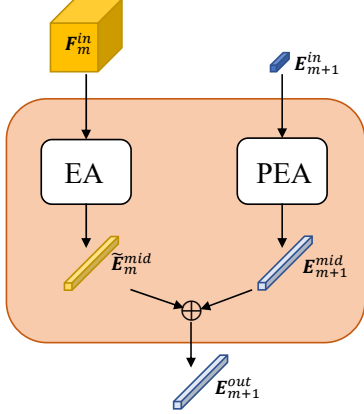


Fig. 5: Combination of Embedding Assistant (EA) and Patch Embedding Alignment (PEA) in Fig. 3(c). The knowledge distillation pipeline through the EA modules and the student transformer blocks can be regarded as a medium-sized pseudo assistant model to provide supplementary distillation streams. F_m^{in} denotes the resulting feature map of the m -th stage, which is processed by the student’s embedding module to output the patch embedding of the next stage E_{m+1}^{in} .

teacher, except for the numbers of hidden states and transformer layers. The number of hidden states is adopted from the student, while the amount of the transformer layers corresponds to the one of the teacher. However, one weak spot of the TA paradigm is its higher computational cost and an additional training stage required for training of the intermediate TA model.

We draw inspiration from the concept of TA but address the aforementioned drawback into account and propose the *Embedding Assistant (EA)* module which serves as a mediator between the teacher and the student *without* requiring two-stage distillation. An overview of the proposed EA module is given in Fig. 3(c). EA is an embedding module whose structure is identical to the one of the student’s and the teacher’s embedding module and with the number of channels C corresponding to the one of the teacher. With the same kernel size of the convolution operation to realize patch embedding, the outputs of EA, PEA, and the teacher’s embedding module have the same number of patches. As shown in Fig. 3(c) and Fig. 5, the results of EA and PEA are fused via element-wise addition stage-by-stage.

Given that a transformer block of the teacher consists of L -transformer layers with an embedding size d_e , and a transformer block of the student consists of M -transformer layers with an embedding size of d'_e , the combination of EA modules and the student’s transformer blocks can be viewed as a pseudo assistant model with a transformer block of M -transformer layers and an embedding size of d_e . Therefore, the medium-sized pseudo assistant model, *i.e.*, the combination of all four stage EAs and student transformer blocks, helps to bridge the student-teacher size gap and provides supplementary information. Since the embedding method of different models varies greatly, the knowledge distillation framework using the proposed EAs does not achieve full plug-and-play flexibility. Yet, compared with the teacher assistant [25], we strengthen the student-teacher distillation without a costly two-step knowledge distillation process.

3.3 Feature Map Distillation

Many knowledge distillation methods deploy a single-stage feature-based scheme for semantic segmentation [14], [18], [19], *i.e.*, the information is exchanged at a single network depth. Our next consideration is that *cross-stage* relation-based knowledge distillation is important for efficient segmentation transformers, as it enables information transfer at across different network depths. Similar ideas have shown success in the past, for example, in the case of hierarchical dense prediction transformers which utilize cross-stage feature maps [22], [23].

We revisit Knowledge Review [15], which studies the connections across different levels of the teacher and the student CNN models. However, the Attention Based Fusion (ABF), which is the original feature map fusion module in Knowledge Review, dynamically aggregates feature maps via a *spatial* attention map, yet, overlooking the channel dimension within the attention maps. We therefore aim to design a complementary channel selection module. Our design is motivated by the following two aspects: 1) The channel-wise cues of the feature maps provide informative priors for feature extractors, and numerous previous works [116], [117], [118] on feature map fusion, seek to fuse spatial and channel information via channel attention. Furthermore, Shu *et al.* [14] indicate that minimizing the channel-wise Kullback-Leibler (KL) divergence of the feature- and prediction maps is more efficient than using the its spatial counterpart. 2) As the patch embedding distillation tracks dependencies among distant spatial positions via sequence-wise learning, the feature map distillation should engage more spatially-holistic knowledge in channels. It is therefore important to highlight channels from certain stages via reweighting and account for cross-stage channel interdependencies. To achieve this, we propose the *Cross Selective Fusion (CSF)* module to adaptively fuse the information across stages via channel attention.

Cross selective fusion. In this module, the feature maps from the current student stage and the next CSF are first resized to a uniform dimensionality and then fused via a channel-wise attention. As shown previously in [116], [118], feature extractions with different kernel sizes or modalities could be fused in an adaptive way. Similarly, we propose to fuse cross-stage feature maps for a relation-based distillation. As shown in Fig. 6, we first conduct a 1×1 convolution to implement the channel-wise transformation of the input feature map F_m^{in} and conduct interpolation to implement the spatial transformation of the feature map F_{m+1}^{mid} from CSF of the next stage. Their height and width are the same as the feature map of the m -th stage F_m^{in} . The resulting \tilde{F}_m^{in} and \tilde{F}_{m+1}^{mid} are element-wise summed, as depicted in Eq. (6):

$$F_m = \tilde{F}_m^{in} + \tilde{F}_{m+1}^{mid}. \quad (6)$$

The global information is then embedded via global average pooling, where s_c denotes the channel-wise statistics, as shown in Eq. (7):

$$s_c = \mathcal{F}_{gp}(F_m) = \frac{1}{H \times W} \sum_{i=1}^H \sum_{j=1}^W F_m(i,j). \quad (7)$$

Then, a compact feature $z \in \mathbb{R}^{d \times 1}$ in Eq. (8) is generated for precise and adaptive selections:

$$z = \mathcal{F}_{fc}(s_c) = \delta(\mathcal{B}(\phi(s_c))), \quad d = \max(C/r, L), \quad (8)$$

where $\delta(\cdot)$ denotes the ReLU function, $\mathcal{B}(\cdot)$ denotes Batch Normalization, and $\phi(\cdot)$ denotes 1×1 convolution. d is the dimension

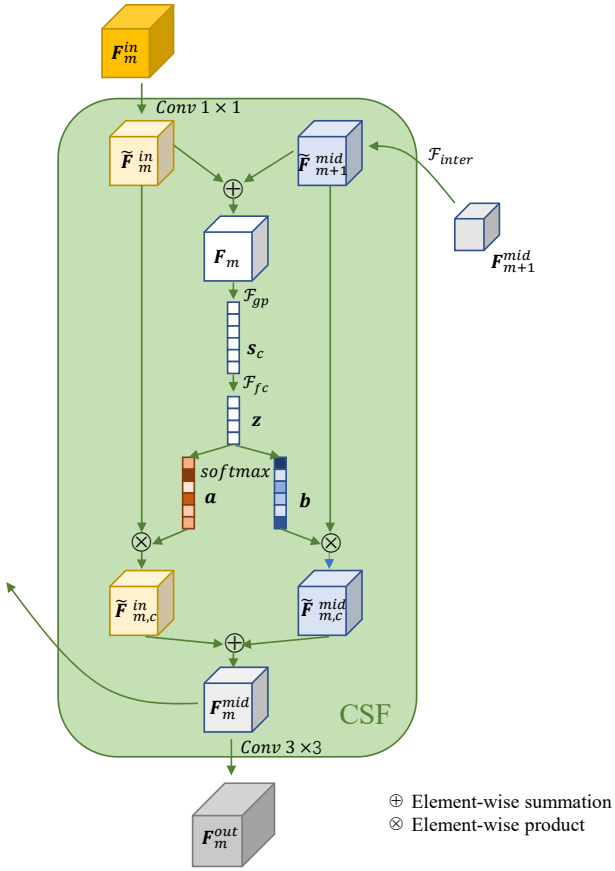


Fig. 6: Architecture of the feature map fusion module, Cross Selective Fusion (CSF) in Fig. 3. The dimension-wise unified feature maps from the current student transformer block and the higher-level features are fused via a channel attention.

of the vector z , which is controlled by a reduction ratio r . L is chosen to be the minimum value of d .

Soft attention across the channels is then used to adaptively select information from different branches:

$$a_c = \frac{e^{\mathbf{A}_c z}}{e^{\mathbf{A}_c z} + e^{\mathbf{B}_c z}}, \quad b_c = \frac{e^{\mathbf{B}_c z}}{e^{\mathbf{A}_c z} + e^{\mathbf{B}_c z}}, \quad (9)$$

$$\mathbf{F}_{m,c}^{mid} = a_c \cdot \tilde{\mathbf{F}}_m^{in} + b_c \cdot \tilde{\mathbf{F}}_{m+1}^{mid}, \quad a_c + b_c = 1, \quad (10)$$

where $\mathbf{A}, \mathbf{B} \in \mathbb{R}^{C \times d}$ are two learnable matrices and $\mathbf{A}_c, \mathbf{B}_c \in \mathbb{R}^{1 \times d}$ are their c -th elements. a_c , b_c , and $\mathbf{F}_{m,c}^{mid}$ are the c -th elements of \mathbf{a} , \mathbf{b} , and $\mathbf{F}_{m,c}^{mid}$. \mathbf{a} and \mathbf{b} denote the soft attention vector for $\tilde{\mathbf{F}}_m^{in}$ and $\tilde{\mathbf{F}}_{m+1}^{mid}$, respectively. Further, we conduct a 3×3 convolution to convert $\mathbf{F}_{m,c}^{mid}$ to $\mathbf{F}_{m,c}^{out}$, which has the same dimension as the teacher's feature map.

Feature map loss function. For training, we compute the HCL loss [15] between the outputs of the CSF and the teacher transformer block at each stage, as shown in Fig. 3. The feature map obtained from CSF at each stage with shape $[n, c, h, w]$ is divided into 4-level context information via adaptive average pooling. The height of the resulting multi-level feature maps at one stage is $[h, 4, 2, 1]$, which denotes that the shapes of the four abstract feature maps are $[n, c, h, w]$, $[n, c, 4, 4]$, $[n, c, 2, 2]$, and $[n, c, 1, 1]$. At each stage, L_2 distances are utilized to distill knowledge between the

context levels. The final HCL loss between the feature maps at the m -th stage is computed as:

$$L_{fm}^m = \frac{1}{1 + \sum_l \frac{1}{2^l}} \sum_{l=0}^3 \frac{1}{2^l} MSE(\mathbf{F}_{m,l}^{out}, \mathbf{F}_{m,l}^T), \quad (11)$$

where l refers to the number of level at one stage. The purpose of placing the HCL loss after every stage is to encourage knowledge distillation at different levels of abstraction.

3.4 Configuration

The core of our TransKD framework involves two knowledge distillation strategies: the patch embedding distillation (described in Sec. 3.2) and the feature map distillation (see Sec. 3.3). To realize this design, we introduce four modules: *PEA*, *GL-Mixer*, and *EA* modules guide the patch embedding distillation, while the *CSF* feature map fusion module enhances the cross-stage relation-based feature map distillation.

Overall, CSF and PEA can be viewed as the fundamental components of TransKD. GL-Mixer operates on the *deepest* representative embedding, (*i.e.*, the final fourth stage) producing highly heterogeneous patterns [22]. It reinforces the patch embedding distillation at the final stage by harvesting global and local context information in two branches. The EA modules are placed *at each stage* and serve as an embedding method to provide supplementary distillation streams by using an identical embedding method to the teacher's and the student's, with the teacher's number of channels. It should be taken into account, that as different transformer architectures have different embedding methods, the framework leveraging EA does not yield full plug-and-play flexibility.

We implement and examine different variants of our proposed framework. Note, that we cannot isolate and verify the efficacy of each module when all the modules are combined together, as an integration of these components means many constraints and could lead to overfitting. We therefore focus on three configurations of the feature map distillation and the patch embedding distillation provided in Tab. 1, which we refer to as *TransKD-Base*, *TransKD-GL*, and *TransKD-EA*. The structure of these three framework variants is provided in Fig. 3.

TABLE 1: Configuration of TransKD variants.

Framework	FM Distillation	PE Distillation	Plug&Play
TransKD-Base	CSF	PEA	✓
TransKD-GL	CSF	PEA+GL-Mixer	✓
TransKD-EA	CSF	PEA+EA	✗

4 EXPERIMENT DATASETS AND SETUPS

4.1 Datasets and Metrics

Cityscapes [27] is a large-scale dataset, which contains stereo video sequences of street scenes from 50 different cities. Cityscapes consists of 2975 training- and 500 validation images with dense annotations as well as 1525 test images. It is well known for assessing the performance of vision algorithms for urban semantic scene understanding. There are 19 semantic classes.

ACDC [28] is a dataset used to address semantic segmentation under adverse conditions, *e.g.*, fog, nighttime, rain, and snow

scenes. Each adverse condition includes 400 training, 100 validation, and 500 test images, except for the nighttime condition which includes 106 validation images. Tougher and more comprehensive situations are characteristic for the ACDC dataset, as its goal is to validate the quality of semantic segmentation under adverse conditions with the identical label set of 19 classes as Cityscapes.

NYU Depth V2 is an indoor dataset captured by both the RGB and depth cameras. It contains scenes of offices, stores, and rooms of houses. There are many occluded objects with uneven illumination. The dataset includes 1449 RGB-depth images, divided into 795 training images and 654 testing images. The images are annotated with 40 semantic categories. We use the RGB images in our experiments investigating knowledge distillation.

Evaluation metric. The mean Intersection over Union (mIoU) over all classes is a common evaluation metric for semantic segmentation tasks. All experiments are evaluated based on mIoU, which is calculated via Eq. (12):

$$mIoU = \frac{1}{k+1} \sum_{i=0}^k \frac{p_{ii}}{\sum_{j=0}^k p_{ij} + \sum_{j=0}^k (p_{ji} - p_{ii})}, \quad (12)$$

where k is the number of classes, p_{ij} is the number of pixels belonging to the class i and classified as class j . We use MMCV¹ to compute FLOPs and the number of parameters of our models.

4.2 Implementation Details

Teacher and student transformer models. For the main part of our semantic segmentation experiments, we investigate knowledge distillation for compressing a large pre-trained SegFormer B2 to a smaller SegFormer B0 model without pre-training (unless specified), which have a similar number of parameters as ResNets used in previous distillation works [12], [14], [15]. SegFormer B0 achieves a speed of 47.6 Frames Per Second (FPS) when running at a resolution of 512×1024 and therefore suits well for real-time applications [22]. We have also examined our framework with PVTv2 [30] and LVT [31] to study the generality of our approach.

Training setups and hyperparameters. When evaluating the performance of the knowledge distillation frameworks, we resize the images to 512×1024 for Cityscapes [27] unless specified and 512×910 for ACDC [28], while the original image scale of 480×640 is kept for the NYUv2 dataset [29]. We use one NVIDIA GTX 1080Ti GPU when experimenting with the aforementioned input sizes and four NVIDIA A100 GPUs for larger input sizes. The number of epochs is set to be 1000 on Cityscapes and ACDC datasets, and 1500 on the NYUv2 dataset. Following the structure of SegFormer [22], the height and width of the output and the target segmentation maps are all rescaled with ratio 1/4 compared to the input image. The performance of the baseline SegFormer model has a slight decay, which is reasonable due to a smaller size of the input image. The models in our work are trained using the AdamW optimizer [119] with a batch size of 2 with the learning rate initialized as 6×10^{-5} and adjusted by a polynomial learning rate decay scheduler with a factor of 1.0 by default. Besides, the number of channels of the feature maps in the CSF fusion module C is set to 64.

5 EXPERIMENT RESULTS AND ANALYSIS

5.1 Quantitative results

Results on the Cityscapes dataset. In Tab. 2, we compare the performance of our TransKD method without pretraining the

TABLE 2: Comparison with knowledge distillation methods on the Cityscapes dataset [27].

Network	#Params (M)	GFLOPs	mIoU (%)
Teacher (B2)	27.36	113.84	76.49
Student (B0)	3.72	13.67	55.86
+Pre-train	3.72	13.67	69.75
+KD [16]	3.72	13.67	56.89
+CD [14]	3.72	13.67	61.90
+SKD (PA) [12]	3.85	13.74	58.05
+SKD (HO) [12]	3.85	13.74	59.00
+Knowledge Review [15]	4.35	16.17	63.40
+TransKD-Base (ours)	4.56	16.47	68.58 (+5.18)
+TransKD-GL (ours)	5.22	16.80	68.87 (+5.47)
+TransKD-EA (ours)	5.53	17.84	68.98 (+5.58)

student model on ImageNet, to a multitude of previously published knowledge distillation approaches, on the Cityscapes validation set. We first validate the usefulness of our framework against a baseline trained without knowledge distillation and see that a student SegFormer-B0 model optimized with our TransKD-EA distillation framework achieves a +13.12% improvement (55.86% vs. 68.98%) in mIoU. TransKD-EA also outperforms other distillation frameworks by a significant margin, for example, +5.58% compared to the feature-map-only distillation approach Knowledge Review (KR) [15], revealing the benefits of unifying patch embedding and feature map distillation. Furthermore, the student model distilled by using TransKD-EA delivers results comparable to the student model with additional lengthy pre-training. We acknowledge, that out knowledge distillation frameworks TransKD-GL and TransKD-EA comprise relatively heavy designs. Still, the lightweight variant of our framework TransKD-Base is alone sufficient to conduct the distillation, yielding a surprising +5.18% gain compared to KR [15].

Comparison against previous distillation methods. Compared to the traditional response-based [16], feature-based [12], [14], and relation-based [15] knowledge distillation, the combination of traditional distillation and patch embedding distillation greatly improves the effectiveness of transformer-to-transformer transfer. Besides, compared to the teacher model which is based on the SegFormer-B2, the student model with SegFormer-B0 backbone reduces >85% GFLOPs. Moreover, TransKD-EA rivals the notoriously time-consuming pre-training method. Note that the number of parameters and GFLOPs listed in Tab. 2 include those of the model itself and those of the distillation framework.

However, at test-time, the computational complexity of the enhanced student model is not affected by the distillation method and is identical to the original compact student model (3.72M parameters and 13.67G FLOPs), therefore keeping the high efficiency needed in real-world applications.

Per-class accuracy analysis on Cityscapes. Next, we investigate the performance of our framework for the individual categories in Tab. 3, comparing the TransKD variants to the feature-map-only distillation baseline Knowledge Review (KR) [15]. TransKD-GL is better at recognizing small infrastructures, such as *traffic light*, *traffic sign*, and *pole*, while the TransKD-EA has better performance on the categories like *wall* and *train*. Both variants surpass the KR framework for all classes with a remarkable gap especially for *wall*, *pole*, *person*, *rider*, *truck*, and *train*. In Fig. 7(a), we further showcase per-class accuracy of the original

1. MMCV: <https://github.com/open-mmlab/mmcv>

TABLE 3: Per-class IoU scores of our proposed knowledge distillation frameworks compared with the feature-map-only baseline distillation method Knowledge Review [15] on the validation set of Cityscapes [27].

Method	mIoU	road	sidewalk	building	wall	fence	pole	traffic light	traffic sign	vegetation
Knowledge Review [15]	63.40	97.09	78.07	88.26	37.55	44.12	46.55	53.15	60.96	89.39
TransKD-Base	68.58	97.47	80.29	89.71	47.13	48.25	53.78	56.24	65.82	90.74
TransKD-GL	68.87	97.59	80.50	89.83	47.87	46.80	54.34	57.97	66.65	90.88
TransKD-EA	68.98	97.46	79.91	89.75	54.37	47.87	53.21	56.06	65.25	90.70
Class	terrain	sky	person	rider	car	truck	bus	train	motorcycle	bicycle
Knowledge Review [15]	57.74	92.34	65.26	40.58	89.83	50.92	64.30	44.29	40.79	63.40
TransKD-Base	60.63	93.05	71.92	45.76	91.84	66.02	74.01	63.31	39.60	67.54
TransKD-GL	62.07	92.73	72.21	46.15	91.88	70.37	67.39	57.18	48.28	67.81
TransKD-EA	60.94	92.59	71.14	45.89	91.61	65.56	71.17	66.96	43.46	66.68

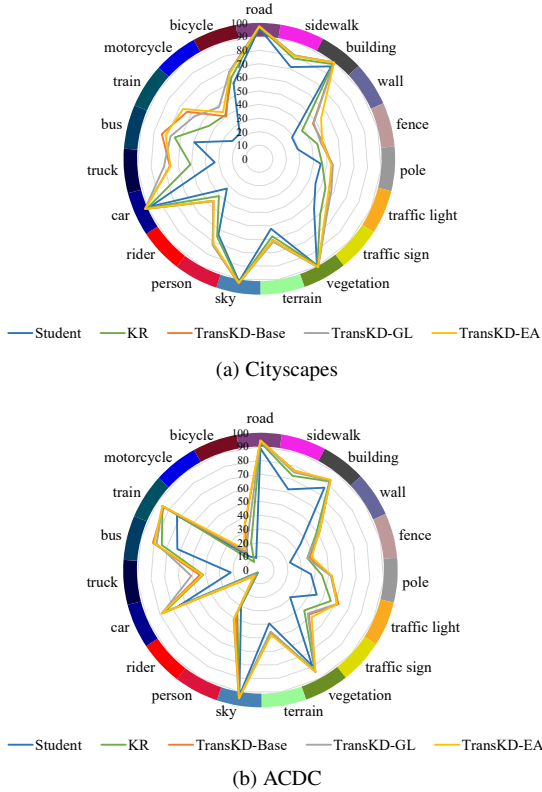


Fig. 7: Semantic segmentation IoUs of our TransKDs compared with non-pretrained student and Knowledge Review [15] on Cityscapes and ACDC datasets.

student model, the KR framework, and our TransKD approaches. The benefits of TransKDs are especially large for the challenging less-frequent vehicle categories such as *bus*, *train*, and *truck*.

Effectiveness for different architectures. We then verify whether the effectiveness of our method is consistent for different architectures. With this intent, we compare the TransKD-Base method against the Knowledge Review (KR) framework [15] for different segmentation backbones on the Cityscapes dataset. The results in Tab. 4 indicate that our approach is not strictly tied to a concrete model, but is consistently beneficial for different segmentation backbones. Specifically, our TransKD-Base method achieves +5.18%, +2.18%, and +2.71% improvements over the feature-map-only KR method, while using the SegFormer-B0, the PVTv2-B0 [30], and the Lite Vision Transformer (LVT) [31] model as the

student, respectively. For the PVTv2-B0, we use PVTv2-B2 [30] as the teacher model. In the setting of using the SegFormer-B2 as the teacher and the LVT as the student (which have rather dissimilar structures), our proposed TransKD framework also clearly improves the segmentation quality. When comparing to the original student segmenter without any distillation, the gains are more evident with 12.72%, 10.34%, and 11.05% in mIoU. These results validate that our TransKD framework can unleash the potential of the efficient transformer model, yielding large segmentation improvements of the compact models.

TABLE 4: Accuracy analysis on various transformer structures.

Network	#Params (M)	GFLOPs	mIoU (%)
Teacher (SegFormer-B2)	27.36	113.84	76.49
Student (SegFormer-B0)	3.72	13.67	55.86
+Knowledge Review	4.35	16.17	63.40
+TransKD-Base (ours)	4.56	16.47	68.58 (+5.18)
Teacher (PVTv2-B2)	29.1	83.14	77.26
Student (PVTv2-B0)	7.53	47.45	58.35
+Knowledge Review	8.15	49.94	66.51
+TransKD-Base (ours)	8.37	50.24	68.69 (+2.18)
Teacher (SegFormer-B2)	27.36	113.84	76.49
Student (LVT)	3.84	18.06	57.49
+Knowledge Review	4.47	20.63	65.83
+TransKD-Base (ours)	4.69	20.99	68.54 (+2.71)

Results on the ACDC dataset. Tab. 5 summarizes the distillation outcome of CD [14], KR [15], and our TransKD approaches on the ACDC validation dataset. Apart from the overall mIoU scores, we examine the models on four different adverse conditions captured in the ACDC dataset, namely *fog*, *night*, *rain*, and *snow*. Our TransKD-EA method obtains the best performance with 59.09% of mIoU on the All-ACDC benchmark, and the top scores of 66.13%, 44.99%, and 57.24% of mIoU for the *fog*, *night*, and *rain* subsets respectively. Interestingly, another variant of our framework, TransKD-GL, yields the best outcome of 60.61% on the *snow* subset of the ACDC dataset. We hypothesize that for snowy scenes, local cues are crucial for segmentation and TransKD-GL excels, due to extraction of detailed information from the representative high-level embedding. Compared to Knowledge Review, all of our three TransKD variants have respective +3.66%, +3.23%, and +4.19% performance gains. The improvements on these diverse weather and nighttime subsets confirm the effectiveness of TransKD for different scene appearances.

Per-class accuracy analysis on ACDC. We also provide the per-class segmentation results of different frameworks on the ACDC

TABLE 5: Accuracy analysis on the ACDC dataset [28] in different adverse conditions.

Network	Fog	Night	Rain	Snow	All-ACDC
Teacher (B2)	73.26	51.44	69.26	72.00	69.34
Student (B0)	52.10	33.33	45.79	48.38	46.26
CD [14]	57.07	40.82	51.37	52.15	52.36
Knowledge Review [15]	59.83	42.38	52.30	55.69	54.90
TransKD-Base (ours)	63.74	44.63	57.16	60.30	58.56 (+3.66)
TransKD-GL (ours)	63.18	43.55	55.85	60.61	58.13 (+3.23)
TransKD-EA (ours)	66.13	44.99	57.24	59.88	59.09 (+4.19)

dataset in Fig. 7(b). Compared to the original student and the KR-boosted student, models optimized with our TransKD approach have evident gains on most classes. In particular, TransKD has substantial improvements on certain categories which take less space (and are thus harder to segment) but are very important for autonomous driving, such as *pole*, *traffic light*, and *traffic sign*.

Results on the NYUv2 dataset. Our next area of investigation are segmentation results for the *indoor* scenes covered by the NYUv2 dataset [29]. The original student model with SegFormer-B0 achieves a relatively low performance of 18.19% in mIoU on NYUv2. While the CD and KR frameworks only bring limited improvements, our TransKD-GL method reaches the best mIoU score of 24.20%. Compared to KR, our TransKD-Base, -GL, and -EA distillation frameworks reach +0.81%, +1.40%, and +1.09% mIoU gains, respectively. This indicates that our TransKD methods are also beneficial for indoor scene understanding.

TABLE 6: Accuracy analysis on the NYUv2 dataset [29].

Network	#Params (M)	GFLOPs	mIoU (%)
Teacher (B2)	27.38	114.37	44.11
Student (B0)	3.72	13.85	18.19
+CD [14]	3.72	13.85	20.83
+Knowledge Review [15]	4.35	16.35	22.80
TransKD-Base (ours)	4.57	16.64	23.61 (+0.81)
TransKD-GL (ours)	5.22	16.98	24.20 (+1.40)
TransKD-EA (ours)	5.54	18.02	23.89 (+1.09)

5.2 Ablation Studies and Comparisons

Effectiveness of feature map fusion module and loss function. The feature map distillation component of TransKD (Sec. 3.3) covers the feature map fusion modules and the loss functions. For robust feature map distillation, we have introduced Cross Selective Fusion (CSF), to substitute the original feature fusion module ABF in Knowledge Review [15]. CSF is based on a channel attention mechanism for transformer feature map distillation. To verify the effectiveness of CSF, we compare CSF and ABF when using the HCL loss function on Cityscapes [27] and ACDC [28] in Tab. 7. It is evident, that CSF clearly outperforms ABF with accuracy gaps of 2.54% and 0.45% on the two datasets. This finding showcases the usefulness of CSF and the importance of channel-wise dependencies for transformer-based knowledge distillation.

We further aim to isolate the role of the feature map loss function in a separate set of experiments, with the results summarized in Tab. 8. The Kullback-Leibler (KL) divergence loss is widely used in knowledge distillation and enables the student to imitate

TABLE 7: Accuracy analysis on the feature map fusion module.

Feature Map Fusion	Loss Function	Dataset	mIoU (%)
ABF [15]	HCL	Cityscapes	63.40
CSF (ours)	HCL	Cityscapes	65.94 (+2.54)
ABF [15]	HCL	ACDC	54.90
CSF (ours)	HCL	ACDC	55.35 (+0.45)

the teacher’s distributions, *i.e.* model predictions [12], [14], [16] or feature maps [14]. Thus, we choose the channel-wise and spatial KL divergence loss functions as control groups for confirming the effectiveness of HCL (the hierarchical version of the MSE loss). The results demonstrate that HCL outperforms both KL divergence losses by >1.5% when distilling the intermediate feature maps.

TABLE 8: Accuracy analysis on the feature map distillation loss function.

Loss Function	Feature Map Fusion	PEA	mIoU (%)
Channel-wise KL	CSF	All	66.80
Spatial-wise KL	CSF	All	66.28
HCL	CSF	All	68.58

Effectiveness of patch embedding distillation. In this paper, patch embedding distillation (Sec. 3.2) is for the first introduced in the field of semantic segmentation. Tab. 9 summarizes our experiments targeting the effects of patch embedding distillation for different stages. When distilling one stage of patch embedding, the patch embedding loss is directly added to the feature map loss, *i.e.*, $\alpha_m = 1$. Patch embedding distillation at any stage is effective, as it clearly boosts the performance compared to its counterparts without knowledge exchange at the patch embedding level. Generally, the deeper the stage, the more channels of the patch embedding are used and the better the distillation effect the framework can provide. Note that the original feature-map-only Knowledge Review does not use any patch embedding distillation and reaches a much lower outcome of 63.40%. Models yield their best performances with all-stage patch embedding distillations in place, *e.g.*, 67.89% in mIoU for Knowledge Review (equipped with our PEA modules) and 68.58% for TransKD.

Additionally, here we use CSF+HCL to represent our feature

TABLE 9: Accuracy analysis on integration of PEA by stages.

Feature Map Distillation	PEA Stage	Channels		mIoU (%)
		Student	Teacher	
Knowledge Review [15]	None	-	-	63.40
	1st	32	64	64.78
	2nd	64	128	65.62
	3rd	160	320	66.37
	4th	256	512	66.52
	All	-	-	67.89
CSF+HCL (TransKD)	None	-	-	65.94
	1st	32	64	66.75
	2nd	64	128	67.05
	3rd	160	320	67.08
	4th	256	512	67.73
	All	-	-	68.58

map distillation part in TransKD-Base and compare it with Knowledge Review combined with PEA. Our CSF+HCL improves the outcome by 1.2%~2.5% over Knowledge Review with different PEA configurations (both when it is not combined or combined with PEA at different stages), verifying the benefits of the proposed feature map fusion module CSF. When the feature map distillation frameworks leverage PEA at all stages with weights of $\alpha = [0.1, 0.1, 0.5, 1]$, CSF+HCL reaches the best mIoU of 68.58% still surpassing the Knowledge Review variant enhanced with our patch embedding distillation blocks by 0.69%.

Influence of weight settings. During our training process, the patch embedding loss and feature map loss at each stage are added to the original cross-entropy loss, resulting in nine loss terms in total. Because of the large number of loss terms, a proper weight setting adjustment is required to boost the performance. In Tab. 10, we compare three weight settings. The first row reveals that distilling patch embeddings and feature maps with equal weights leads to overfitting, resulting a sub-optimal mIoU score of 67.75%. As described in Tab. 9 and previous studies [12], [14], modelling deeper patch embeddings and feature maps with more channels and abstract information helps to enhance the knowledge distillation process. In order to reduce the constraints, we experiment by setting either the weights of patch embedding loss or the weights of feature map loss to be [0.1, 0.1, 0.5, 1].

TABLE 10: Distillation with different weights. “FM”: Feature Map; “PE”: Patch Embedding.

Framework	FM Weights	PE Weights	mIoU (%)
TransKD-Base	[1,1,1,1]	[1,1,1,1]	67.75
	[1,1,1,1]	[0.1,0.1,0.5,1]	68.58
	[0.1,0.1,0.5,1]	[1,1,1,1]	66.48

We see in Tab. 10 that the performance is improved by reducing the weights of the low-level patch embeddings, whereas reducing the weights of the shallower feature maps causes incomplete distillation. Thus, we use the identified best weight setting for TransKD in the following experiments.

Influence of input size and pre-training weights. According to the original work [22], using large input images significantly improves the segmentation results of SegFormer. Besides, ImageNet pre-training is a ubiquitous way for transformer-based methods to compensate for the lack of inductive bias and speed up the convergence. In Tab. 11, we examine the influence of the input size and pre-trained weights by comparing the results of Knowledge Review [15] and TransKD-Base for different configurations.

We first look at the networks *without* weight initialization via pre-training, (*i.e.*, without “+ImN” in Tab. 11). In this case, large image scale facilitates the efficacy of the overall semantic segmentation model while compromising the gain of TransKD relative to Knowledge Review and the student. At the image size of 512×1024 , TransKD-distilled student raises the accuracy by 12.72% compared to the original non-pretrained student. With the full size of 1024×2048 , our TransKD-Base attains the performance of 71.59% with a less, yet still significant accuracy increase of 9.73% in mIoU. As expected, larger input size leads to better results for both, the pre-trained and the non-pretrained networks. We believe, that since pre-training on a large dataset is supposed to complement the inductive bias, and the proposed patch embedding distillation follows the same purpose, TransKD-Base outperforms Knowledge Review by a smaller margin when the students are pre-

TABLE 11: Accuracy analysis on different sizes of input images. KR: Knowledge Review [15]. “ImN” indicates knowledge distillation is conducted on students with ImageNet pre-trained weights.

Input Size	Network	mIoU (%)
512×1024	Teacher (SegFormer-B2)	76.49
	Student (SegFormer-B0)	55.86
	+KR	63.40
	+TransKD-Base (ours)	68.58 (+5.18)
	+ImN	69.75
	+KR+ImN	71.63
768×1536	+TransKD-Base+ImN	71.84
	Teacher (SegFormer-B2)	78.50
	Student (SegFormer-B0)	59.61
	+KR	67.97
	+TransKD-Base (ours)	70.93 (+2.96)
	+ImN	73.07
1024×2048	+KR+ImN	73.84
	+TransKD-Base+ImN	74.06
	Teacher (SegFormer-B2)	79.90
	Student (SegFormer-B0)	61.86
	+KR	69.06
	+TransKD-Base (ours)	71.59 (+2.53)
	+ImN	73.77
	+KR+ImN	75.55
	+TransKD-Base+ImN	75.74

trained. Unsurprisingly, the best semantic segmentation quality is achieved when fine-tuning the student pre-trained on ImageNet with our TransKD-Base knowledge distillation approach, yielding 75.74% in mIoU.

Comparison to state-of-the-art segmenters. In Tab. 12, we further compare TransKD-Base against state-of-the-art semantic segmentation networks and previous knowledge distillation methods. While heavier models like CCNet [41] and SETR [7] reach high mIoU scores, they are computationally intensive, which often disqualifies their deployment in mobile and real-time systems. Accurate segmenters like HANet [121] and SegFormer-B5 [22] require $>1000G$ FLOPs to yield precise high-resolution predictions. We further consider more efficient semantic segmenters. Compact models, such as CGNet [124] and Fast-SCNN [63], are very lightweight but come at a high accuracy cost and the segmentation quality declines. Some models with moderate computation complexity like ERFNet [3] and BiSeNet [62] can attain higher accuracy, but also comprise more model parameters.

Our previous experiments in Sec. 5.1 examined different knowledge distillation methods with the same student backbone. In this section, we conduct more comparisons to previously published methods with numbers from their respective papers for the enhanced student after distillation (Tab. 12). Most of the previous works have used PSPNet18 [24] as the student model. In the group of distillation methods and non-pretrained students, our TransKD-Base yields top performance of 71.59% in mIoU, which is even close to the results of some pre-trained students, *e.g.*, MD [126] (71.90%). In the group of distillation methods and pre-trained students, TransKD achieves the highest mIoU score despite being the most lightweight model with only 3.72M parameters and 54.70G FLOPs. Fig. 8 visualizes the comparison of representative efficient segmentation models and knowledge distillation methods. We clearly see that TransKD stands out in front of the past state-of-the-art models in both groups and

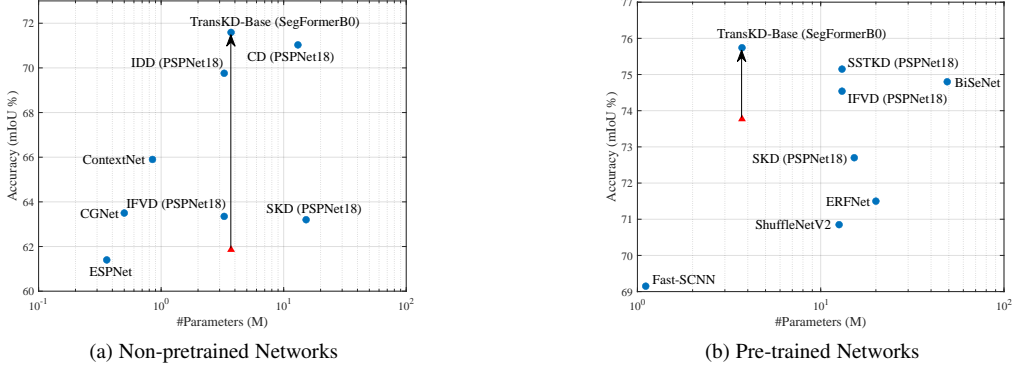


Fig. 8: Comparison between TransKD and state-of-the-art efficient semantic segmentation networks and knowledge distillation methods, in terms of (a) not using pre-trained weights and (b) using pre-trained weights. TransKD greatly boosts the mIoU of the efficient model.

TABLE 12: Performance comparison with state-of-the-art distillation methods over different student segmentation networks on the Cityscapes validation set [27]. * denotes that the efficient segmentation model uses pre-trained weights. “-” denotes that the corresponding information is missing in the respective paper.

Network	#Params (M)	GFLOPs	mIoU (%)
Large Semantic Segmentation Models			
PSPNet [24]	68.10	-	78.50
DeepLabV3+ [36]	62.70	-	80.90
EncNet [120]	55.10	-	76.90
DANet [40]	45.16	397.40	78.32
CCNet [41]	68.90	-	80.20
HANet [121]	65.40	2138.02	80.29
OCRNet [122]	70.50	-	81.10
SETR-MLA [7]	92.59	-	78.98
SETR-PUP [7]	97.64	-	79.45
MaskFormer [57]	60.00	-	78.50
SegFormer-B4 [22]	64.10	1240.60	82.30
SegFormer-B5 [22]	84.70	1460.40	82.40
Efficient Semantic Segmentation Models			
ERFNNet [3]*	20.00	27.70	71.50
ICNet (Res18)* [61]	26.50	28.30	67.70
ESPNet [13]	0.36	4.42	61.40
BiSeNet (Res18)* [62]	49.00	-	74.80
ContextNet [123]	0.85	-	65.90
SwiftNet (Res18)* [65]	11.80	26.00	70.20
CGNet [124]	0.50	6.00	63.50
Fast-SCNN* [63]	1.11	-	69.15
MobileNetV2* [67]	14.80	142.74	73.93
ShuffleNetV2* [68]	12.60	117.09	70.85
EfficientNet-B0 [125]	4.19	7.97	58.37
SegFormer-B0 (our student)	3.72	54.70	61.86
SegFormer-B0* (our student)	3.72	54.70	73.77
Distillation Methods on Students without using Pretrained Weights			
SKD (PSPNet18) [12]	15.24	128.20	63.20
IFVD (PSPNet18) [18]	3.27	31.53	63.35
CD (PSPNet18) [14]	13.07	125.80	71.03
IDD (PSPNet18) [103]	3.27	31.53	69.76
TransKD-Base (SegFormer B0)	3.72	54.70	71.59
Distillation Methods on Students with Pretrained Weights			
MD* [126]	14.35	64.48	71.90
SKD (PSPNet18)* [12]	15.24	128.20	72.70
KA (PSPNet18)* [106]	16.31	148.20	74.59
IFVD (PSPNet18)* [18]	13.07	125.80	74.54
DSD (PSPNet18)* [20]	15.20	56.90	73.21
SASD (PSPNet)* [21]	11.38	117.26	73.10
CD (PSPNet18)* [14]	13.07	125.80	74.58
APD (PSPNet18)* [107]	16.31	148.20	75.68
SSTKD (PSPNet18)* [19]	13.07	125.80	75.15
CIRKD (PSPNet18)* [102]	12.90	507.40	74.73
TransKD-Base (SegFormer B0)*	3.72	54.70	75.74

strikes an excellent trade-off between efficiency and accuracy for semantic scene understanding.

5.3 Qualitative Results

Analyses of t-SNE visualizations. We next consider the representation point of view and asses the discriminability of the learned embeddings in the latent space via t-SNE visualizations [127] given in Fig. 9, where Fig. 9(a) illustrates the original student embeddings, and Fig. 9(b) and Fig. 9(c) are the student representations learned with KR [15] and our TransKD-Base, respectively.

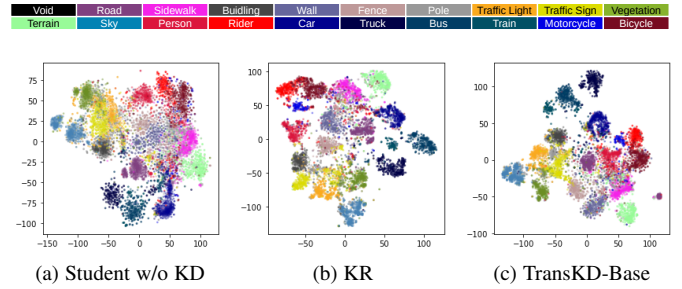


Fig. 9: t-SNE visualisation of the feature maps at the last stage. A random sampling of five hundred feature nodes is taken in each categories. The prediction maps are down-sampled to label the feature nodes semantically.

Without any knowledge distillation, the decision boundaries for most of the categories are obscure and difficult to distinguish, which leads to harder decision making for the classifier. Training with Knowledge Review helps to distinguish most of the categories, but *traffic sign* and *traffic light*, which are crucial for autonomous vehicles, are easily confused. Finally, these issues are better addressed by utilizing our TransKD knowledge distillation. Compared to Fig. 9(a) and Fig. 9(b), we observe clearer inter-category boundaries in Fig. 9(c), which indicates the benefits of the proposed methods unifying patch embedding- and feature distillation as it enhances the discriminability in the latent space. With TransKD, important segmentation cues coming from the teacher model can be well learned by the student model at both patch embedding and feature map levels.

Analyses of intermediate feature maps. Next, we provide visual explanations of the network’s internal decision processes by visualizing the feature maps coming from the 4th stage of the model

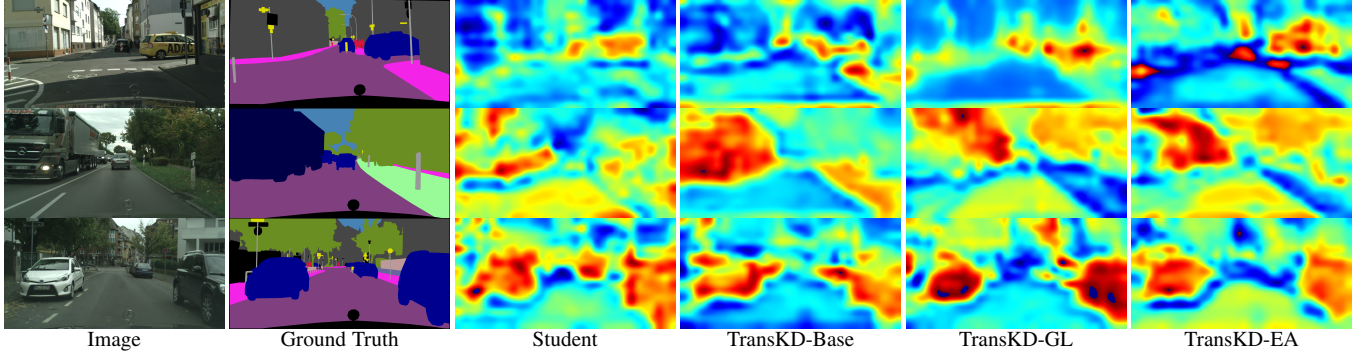


Fig. 10: Feature map visualizations. The feature maps at the last transformer encoder stage, *i.e.*, the 4th stage, are visualized for analysis.



Fig. 11: Qualitative street scene semantic segmentation results under normal condition from the Cityscapes dataset [27] and adverse conditions from the ACDC dataset [28] including fog, night, rain, and snow conditions. The performances of our knowledge distillation frameworks, TransKDs, are compared with Channel-wise Knowledge Distillation (CD) [14] and Knowledge Review (KR) [15].

in Fig. 10, with representative Cityscapes validation set examples. Compared with the student without any TransKD components, TransKD-enhanced models present semantically recognizable responses. TransKD helps to pay more attention on the *car* and *truck* objects, as shown in the reddish regions on the feature maps, while maintaining clear boundaries with the background triggering much weaker feature map responses (blue and green regions), leading to better semantic segmentation outcome. Apart from that, TransKD-Base tends to focus on large objects, *e.g.*, on the *truck*, while TransKD-GL shows more evident responses on *cars* which have relatively smaller size, which we attribute to the extraction of both local and global cues encouraged by this approach. Moreover, TransKD-EA better spotlights the objects which are far away from the camera, *e.g.*, the *car* in the first row. These visualization results further illustrate the effectiveness of TransKD for learning semantic-aware intermediate representations.

Analyses of street scene segmentation. Qualitative results of semantic segmentation in street scenarios under different kinds of weather conditions are depicted in Fig. 11, where normal, foggy, nighttime, rainy, and snowy weathers are considered from left to right in each row. The samples come from Cityscapes (normal weather) and ACDC (adverse weathers), respectively. We compare TransKD variants against the feature-map-only Knowledge Review (KR) [15] and Channel-wise Distillation (CD) [14]. The challenging parts of each example are highlighted with the yellow dashed rectangles. For the example featuring normal-weather yet a complex scene (the *bus* occluded by *traffic signs*), a large amount of false predictions on small objects show up in the student’s result without distillation, while similar unsatisfactory segmentation maps can be also found in CD and KR’s outcomes, *e.g.*, part of the *bus* is wrongly classified as *buildings*. Fortunately, these issues are better addressed by TransKD approaches, leading to complete and much clearer segmentation and demonstrating the its efficacy in dealing with details.

These findings are also confirmed in our experiments featuring different weather conditions of the ACDC benchmark. In the foggy, nighttime, and rainy scenes, TransKD enables better detection of challenging small objects like safety-critical *pedestrians*, as well as *traffic lights* and *traffic signs*. In the snowy scene, TransKD can also parse the *vegetation* despite of this class having similar textures as the background *buildings*, thanks to the embedding distillation transferring long-range dependencies. This again highlights the potential of linking patch embedding- and feature map distillation via our TransKD framework, which derives more informative knowledge than the feature-level-only distillation approaches such as CD and KR.

Analyses of indoor semantic segmentation. In our final study, we turn to the *indoor* semantic segmentation results and illustrate the segmentation outcomes on the NYUv2 dataset [29] in Fig. 12. Compared with the segmentation results produced by the student without any distillation, the segmentation boundaries of TransKD are much clearer, and most of the details of the indoor scenes are preserved, especially for the bedroom scene, *e.g.*, on *pillow*. For the bathroom example, similar results can be found, where, for example, *towel* is better recognized by our approaches. Apart from the objects with relatively small size, objects with less texture cues can be completely segmented, *e.g.*, the *wall* in the bedroom. These qualitative examples consistently confirm good generalization of TransKD across diverse environments (indoor and outdoor, different weather conditions, *etc.*) as well as the benefits of knowledge transfer from both patch embeddings and

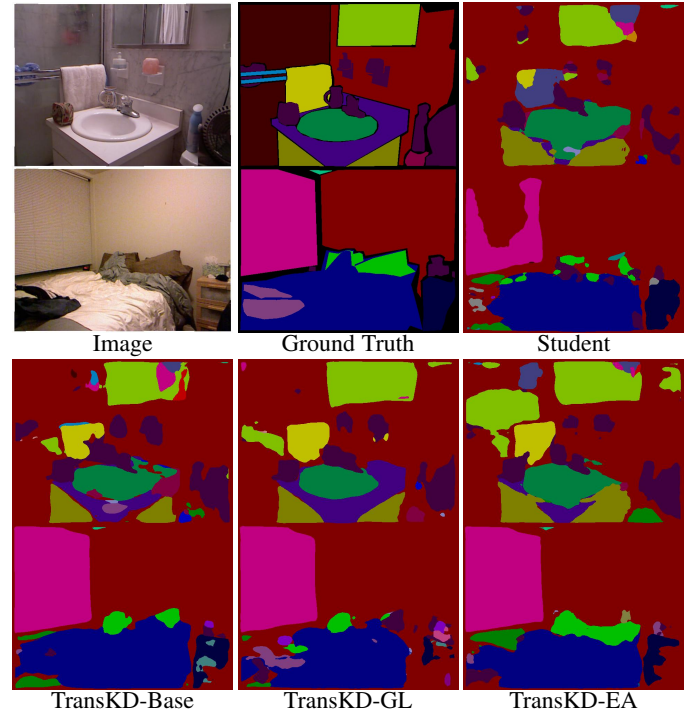


Fig. 12: Qualitative indoor scene semantic segmentation results of our TransKD methods on the NYUv2 dataset [29].

feature maps in transformer-to-transformer knowledge distillation.

6 CONCLUSION

In this work, we target efficient semantic segmentation via transformer-based knowledge distillation. We propose the TransKD architecture, which is the first transformer-to-transformer knowledge distillation framework leveraging transformer-specific patch embeddings as an essential knowledge source. TransKD learns efficient compact segmenters via feature map distillation and patch embedding distillation, with two fundamental modules, *i.e.*, CSF and PEA, and two optimization techniques, *i.e.*, GL-Mixer and EA. To illustrate the performance of the proposed TransKD method, in-depth evaluations are conducted on Cityscapes, ACDC, and NYUv2 datasets with TransKD yielding state-of-the-art performance compared to the existing knowledge distillation approaches. Our experiments provide encouraging evidence, that the proposed transformer-specific patch embedding-level modules are powerful knowledge distillation sources in semantic segmentation with high potential for becoming the foundation of resource-efficient, yet accurate scene understanding models.

In the future, we plan to delve deeper into transformer knowledge distillation by utilizing multi-modal data and make one step further towards transformer-based knowledge factorization, which has been underresearched in semantic segmentation tasks.

ACKNOWLEDGMENTS

This work was supported in part by the Federal Ministry of Labor and Social Affairs (BMAS) through the AccessibleMaps project under Grant 01KM151112, in part by the University of Excellence through the “KIT Future Fields” project, in part by the Helmholtz Association Initiative and Networking Fund on the HAICORE@KIT partition, and in part by Hangzhou SurImage Technology Company Ltd.

REFERENCES

[1] A. Milan, T. Pham, K. Vijay, D. Morrison, A. W. Tow, L. Liu, J. Erskine, R. Grinover, A. Gurman, T. Hunn, N. Kelly-Boxall, D. Lee, M. McTaggart, G. Rallo, A. Razjigaev, T. Rountree, T. Shen, R. Smith, S. Wade-McCue, Z. Zhuang, C. F. Lehnert, G. Lin, I. D. Reid, P. I. Corke, and J. Leitner, “Semantic segmentation from limited training data,” in *ICRA*, 2018.

[2] S. Ainetter and F. Fraundorfer, “End-to-end trainable deep neural network for robotic grasp detection and semantic segmentation from RGB,” in *ICRA*, 2021.

[3] E. Romera, J. M. Alvarez, L. M. Bergasa, and R. Arroyo, “ERFNet: Efficient residual factorized ConvNet for real-time semantic segmentation,” *T-ITS*, vol. 19, no. 1, pp. 263–272, 2018.

[4] K. Yang, X. Hu, Y. Fang, K. Wang, and R. Stiefelhagen, “Omnisupervised omnidirectional semantic segmentation,” *T-ITS*, vol. 23, no. 2, pp. 1184–1199, 2022.

[5] J. Zhang, K. Yang, A. Constantinescu, K. Peng, K. Müller, and R. Stiefelhagen, “Trans4Trans: Efficient transformer for transparent object and semantic scene segmentation in real-world navigation assistance,” *T-ITS*, 2022.

[6] H. Liu, R. Liu, K. Yang, J. Zhang, K. Peng, and R. Stiefelhagen, “HIDA: Towards holistic indoor understanding for the visually impaired via semantic instance segmentation with a wearable solid-state LiDAR sensor,” in *ICCVW*, 2021.

[7] S. Zheng, J. Lu, H. Zhao, X. Zhu, Z. Luo, Y. Wang, Y. Fu, J. Feng, T. Xiang, P. H. S. Torr, and L. Zhang, “Rethinking semantic segmentation from a sequence-to-sequence perspective with transformers,” in *CVPR*, 2021.

[8] R. Strudel, R. Garcia, I. Laptev, and C. Schmid, “Segmenter: Transformer for semantic segmentation,” in *ICCV*, 2021.

[9] A. Dosovitskiy, L. Beyer, A. Kolesnikov, D. Weissenborn, X. Zhai, T. Unterthiner, M. Dehghani, M. Minderer, G. Heigold, S. Gelly, J. Uszkoreit, and N. Houlsby, “An image is worth 16x16 words: Transformers for image recognition at scale,” in *ICLR*, 2021.

[10] A. Vaswani, N. Shazeer, N. Parmar, J. Uszkoreit, L. Jones, A. N. Gomez, Ł. Kaiser, and I. Polosukhin, “Attention is all you need,” in *NeurIPS*, 2017.

[11] J. Deng, W. Dong, R. Socher, L.-J. Li, K. Li, and L. Fei-Fei, “ImageNet: A large-scale hierarchical image database,” in *CVPR*, 2009.

[12] Y. Liu, K. Chen, C. Liu, Z. Qin, Z. Luo, and J. Wang, “Structured knowledge distillation for semantic segmentation,” in *CVPR*, 2019.

[13] S. Mehta, M. Rastegari, A. Caspi, L. Shapiro, and H. Hajishirzi, “ESPNet: Efficient spatial pyramid of dilated convolutions for semantic segmentation,” in *ECCV*, 2018.

[14] C. Shu, Y. Liu, J. Gao, Z. Yan, and C. Shen, “Channel-wise knowledge distillation for dense prediction,” in *ICCV*, 2021.

[15] P. Chen, S. Liu, H. Zhao, and J. Jia, “Distilling knowledge via knowledge review,” in *CVPR*, 2021.

[16] G. Hinton, O. Vinyals, and J. Dean, “Distilling the knowledge in a neural network,” *arXiv preprint arXiv:1503.02531*, 2015.

[17] J. Gou, B. Yu, S. J. Maybank, and D. Tao, “Knowledge distillation: A survey,” *IJCV*, vol. 129, no. 6, pp. 1789–1819, 2021.

[18] Y. Wang, W. Zhou, T. Jiang, X. Bai, and Y. Xu, “Intra-class feature variation distillation for semantic segmentation,” in *ECCV*, 2020.

[19] D. Ji, H. Wang, M. Tao, J. Huang, X.-S. Hua, and H. Lu, “Structural and statistical texture knowledge distillation for semantic segmentation,” in *CVPR*, 2022.

[20] Y. Feng, X. Sun, W. Diao, J. Li, and X. Gao, “Double similarity distillation for semantic image segmentation,” *TIP*, vol. 30, pp. 5363–5376, 2021.

[21] S. An, Q. Liao, Z. Lu, and J.-H. Xue, “Efficient semantic segmentation via self-attention and self-distillation,” *T-ITS*, 2022.

[22] E. Xie, W. Wang, Z. Yu, A. Anandkumar, J. M. Alvarez, and P. Luo, “SegFormer: Simple and efficient design for semantic segmentation with transformers,” in *NeurIPS*, 2021.

[23] W. Wang, E. Xie, X. Li, D.-P. Fan, K. Song, D. Liang, T. Lu, P. Luo, and L. Shao, “Pyramid vision transformer: A versatile backbone for dense prediction without convolutions,” in *ICCV*, 2021.

[24] H. Zhao, J. Shi, X. Qi, X. Wang, and J. Jia, “Pyramid scene parsing network,” in *CVPR*, 2017.

[25] S. I. Mirzadeh, M. Farajtabar, A. Li, N. Levine, A. Matsukawa, and H. Ghasemzadeh, “Improved knowledge distillation via teacher assistant,” in *AAAI*, 2020.

[26] T. Huang, S. You, F. Wang, C. Qian, and C. Xu, “Knowledge distillation from a stronger teacher,” *arXiv preprint arXiv:2205.10536*, 2022.

[27] M. Cordts, M. Omran, S. Ramos, T. Rehfeld, M. Enzweiler, R. Benenson, U. Franke, S. Roth, and B. Schiele, “The cityscapes dataset for semantic urban scene understanding,” in *CVPR*, 2016.

[28] C. Sakaridis, D. Dai, and L. Van Gool, “ACDC: The adverse conditions dataset with correspondences for semantic driving scene understanding,” in *ICCV*, 2021.

[29] N. Silberman, D. Hoiem, P. Kohli, and R. Fergus, “Indoor segmentation and support inference from RGBD images,” in *ECCV*, 2012.

[30] W. Wang, E. Xie, X. Li, D.-P. Fan, K. Song, D. Liang, T. Lu, P. Luo, and L. Shao, “PVT v2: Improved baselines with pyramid vision transformer,” *CVM*, vol. 8, no. 3, pp. 415–424, 2022.

[31] C. Yang, Y. Wang, J. Zhang, H. Zhang, Z. Wei, Z. Lin, and A. Yuille, “Lite vision transformer with enhanced self-attention,” in *CVPR*, 2022.

[32] J. Long, E. Shelhamer, and T. Darrell, “Fully convolutional networks for semantic segmentation,” in *CVPR*, 2015.

[33] V. Badrinarayanan, A. Kendall, and R. Cipolla, “SegNet: A deep convolutional encoder-decoder architecture for image segmentation,” *TPAMI*, vol. 39, no. 12, pp. 2481–2495, 2017.

[34] L.-C. Chen, G. Papandreou, I. Kokkinos, K. Murphy, and A. L. Yuille, “DeepLab: Semantic image segmentation with deep convolutional nets, atrous convolution, and fully connected CRFs,” *TPAMI*, vol. 40, no. 4, pp. 834–848, 2018.

[35] F. Yu and V. Koltun, “Multi-scale context aggregation by dilated convolutions,” in *ICLR*, 2016.

[36] L.-C. Chen, Y. Zhu, G. Papandreou, F. Schroff, and H. Adam, “Encoder-decoder with atrous separable convolution for semantic image segmentation,” in *ECCV*, 2018.

[37] J. Wang, K. Sun, T. Cheng, B. Jiang, C. Deng, Y. Zhao, D. Liu, Y. Mu, M. Tan, X. Wang, W. Liu, and B. Xiao, “Deep high-resolution representation learning for visual recognition,” *TPAMI*, vol. 43, no. 10, pp. 3349–3364, 2021.

[38] Q. Hou, L. Zhang, M.-M. Cheng, and J. Feng, “Strip pooling: Rethinking spatial pooling for scene parsing,” in *CVPR*, 2020.

[39] X. Wang, R. Girshick, A. Gupta, and K. He, “Non-local neural networks,” in *CVPR*, 2018.

[40] J. Fu, J. Liu, H. Tian, Y. Li, Y. Bao, Z. Fang, and H. Lu, “Dual attention network for scene segmentation,” in *CVPR*, 2019.

[41] Z. Huang, X. Wang, L. Huang, C. Huang, Y. Wei, and W. Liu, “CCNet: Criss-cross attention for semantic segmentation,” in *ICCV*, 2019.

[42] Y. Yuan, L. Huang, J. Guo, C. Zhang, X. Chen, and J. Wang, “OCNet: Object context for semantic segmentation,” *IJCV*, vol. 129, no. 8, pp. 2375–2398, 2021.

[43] Y. Liu, Y. Chen, P. Lasang, and Q. Sun, “Covariance attention for semantic segmentation,” *TPAMI*, vol. 44, no. 4, pp. 1805–1818, 2022.

[44] Z. Li, Y. Sun, L. Zhang, and J. Tang, “CTNet: Context-based tandem network for semantic segmentation,” *TPAMI*, 2021.

[45] G. Lin, A. Milan, C. Shen, and I. Reid, “RefineNet: Multi-path refinement networks for high-resolution semantic segmentation,” in *CVPR*, 2017.

[46] C. Yu, J. Wang, C. Gao, G. Yu, C. Shen, and N. Sang, “Context prior for scene segmentation,” in *CVPR*, 2020.

[47] H. Zhao, Y. Zhang, S. Liu, J. Shi, C. C. Loy, D. Lin, and J. Jia, “PSANet: Point-wise spatial attention network for scene parsing,” in *ECCV*, 2018.

[48] T. Takikawa, D. Acuna, V. Jampani, and S. Fidler, “Gated-SCNN: Gated shape CNNs for semantic segmentation,” in *ICCV*, 2019.

[49] H. Ding, X. Jiang, A. Q. Liu, N. M. Thalmann, and G. Wang, “Boundary-aware feature propagation for scene segmentation,” in *ICCV*, 2019.

[50] X. Li, X. Li, L. Zhang, G. Cheng, J. Shi, Z. Lin, S. Tan, and Y. Tong, “Improving semantic segmentation via decoupled body and edge supervision,” in *ECCV*, 2020.

[51] H. Touvron, M. Cord, M. Douze, F. Massa, A. Sablayrolles, and H. Jégou, “Training data-efficient image transformers & distillation through attention,” in *ICML*, 2021.

[52] W. Yu, M. Luo, P. Zhou, C. Si, Y. Zhou, X. Wang, J. Feng, and S. Yan, “MetaFormer is actually what you need for vision,” in *CVPR*, 2022.

[53] J. Gu, H. Kwon, D. Wang, W. Ye, M. Li, Y.-H. Chen, L. Lai, V. Chandra, and D. Z. Pan, “Multi-scale high-resolution vision transformer for semantic segmentation,” in *CVPR*, 2022.

[54] I. O. Tolstikhin, N. Houlsby, A. Kolesnikov, L. Beyer, X. Zhai, T. Unterthiner, J. Yung, A. Steiner, D. Keysers, J. Uszkoreit, M. Lucic, and A. Dosovitskiy, “MLP-mixer: An all-MLP architecture for vision,” in *NeurIPS*, 2021.

[55] Q. Hou, Z. Jiang, L. Yuan, M.-M. Cheng, S. Yan, and J. Feng, “Vision permutator: A permutable MLP-like architecture for visual recognition,” *TPAMI*, 2022.

[56] N. Carion, F. Massa, G. Synnaeve, N. Usunier, A. Kirillov, and S. Zagoruyko, “End-to-end object detection with transformers,” in *ECCV*, 2020.

[57] B. Cheng, A. Schwing, and A. Kirillov, “Per-pixel classification is not all you need for semantic segmentation,” in *NeurIPS*, 2021.

[58] H. Wang, Y. Zhu, H. Adam, A. Yuille, and L.-C. Chen, “MaX-DeepLab: End-to-end panoptic segmentation with mask transformers,” in *CVPR*, 2021.

[59] B. Cheng, I. Misra, A. G. Schwing, A. Kirillov, and R. Girdhar, “Masked-attention mask transformer for universal image segmentation,” in *CVPR*, 2022.

[60] A. Paszke, A. Chaurasia, S. Kim, and E. Culurciello, “ENet: A deep neural network architecture for real-time semantic segmentation,” *arXiv preprint arXiv:1606.02147*, 2016.

[61] H. Zhao, X. Qi, X. Shen, J. Shi, and J. Jia, “ICNet for real-time semantic segmentation on high-resolution images,” in *ECCV*, 2018.

[62] C. Yu, J. Wang, C. Peng, C. Gao, G. Yu, and N. Sang, “BiSeNet: Bilateral segmentation network for real-time semantic segmentation,” in *ECCV*, 2018.

[63] R. P. K. Poudel, S. Liwicki, and R. Cipolla, “Fast-SCNN: Fast semantic segmentation network,” in *BMVC*, 2019.

[64] M. Fan, S. Lai, J. Huang, X. Wei, Z. Chai, J. Luo, and X. Wei, “Rethinking BiSeNet for real-time semantic segmentation,” in *CVPR*, 2021.

[65] M. Orsic, I. Kreso, P. Bevandic, and S. Segvic, “In defense of pre-trained ImageNet architectures for real-time semantic segmentation of road-driving images,” in *CVPR*, 2019.

[66] H. Li, P. Xiong, H. Fan, and J. Sun, “DFANet: Deep feature aggregation for real-time semantic segmentation,” in *CVPR*, 2019.

[67] M. Sandler, A. Howard, M. Zhu, A. Zhmoginov, and L.-C. Chen, “MobileNetV2: Inverted residuals and linear bottlenecks,” in *CVPR*, 2018.

[68] N. Ma, X. Zhang, H.-T. Zheng, and J. Sun, “ShuffleNet V2: Practical guidelines for efficient CNN architecture design,” in *ECCV*, 2018.

[69] X. Li, A. You, Z. Zhu, H. Zhao, M. Yang, K. Yang, S. Tan, and Y. Tong, “Semantic flow for fast and accurate scene parsing,” in *ECCV*, 2020.

[70] T. Verelst and T. Tuytelaars, “SegBlocks: Block-based dynamic resolution networks for real-time segmentation,” *TPAMI*, 2022.

[71] W. Zhang, Z. Huang, G. Luo, T. Chen, X. Wang, W. Liu, G. Yu, and C. Shen, “TopFormer: Token pyramid transformer for mobile semantic segmentation,” in *CVPR*, 2022.

[72] D. Zhou, Z. Yu, E. Xie, C. Xiao, A. Anandkumar, J. Feng, and J. M. Alvarez, “Understanding the robustness in vision transformers,” in *ICML*, 2022.

[73] C. Si, W. Yu, P. Zhou, Y. Zhou, X. Wang, and S. Yan, “Inception transformer,” *arXiv preprint arXiv:2205.12956*, 2022.

[74] Y. Rao, Z. Liu, W. Zhao, J. Zhou, and J. Lu, “Dynamic spatial sparsification for efficient vision transformers and convolutional neural networks,” *arXiv preprint arXiv:2207.01580*, 2022.

[75] L. Yuan, Y. Chen, T. Wang, W. Yu, Y. Shi, Z.-H. Jiang, F. E. Tay, J. Feng, and S. Yan, “Tokens-to-token ViT: Training vision transformers from scratch on ImageNet,” in *ICCV*, 2021.

[76] Z. Liu, Y. Lin, Y. Cao, H. Hu, Y. Wei, Z. Zhang, S. Lin, and B. Guo, “Swin transformer: Hierarchical vision transformer using shifted windows,” in *ICCV*, 2021.

[77] X. Chu, Z. Tian, Y. Wang, B. Zhang, H. Ren, X. Wei, H. Xia, and C. Shen, “Twins: Revisiting the design of spatial attention in vision transformers,” in *NeurIPS*, 2021.

[78] K. Li, Y. Wang, J. Zhang, P. Gao, G. Song, Y. Liu, H. Li, and Y. Qiao, “UniFormer: Unifying convolution and self-attention for visual recognition,” *arXiv preprint arXiv:2201.09450*, 2022.

[79] X. Chu, Z. Tian, B. Zhang, X. Wang, X. Wei, H. Xia, and C. Shen, “Conditional positional encodings for vision transformers,” *arXiv preprint arXiv:2102.10882*, 2021.

[80] R. Ranftl, A. Bochkovskiy, and V. Koltun, “Vision transformers for dense prediction,” in *ICCV*, 2021.

[81] Y. Yuan, R. Fu, L. Huang, W. Lin, C. Zhang, X. Chen, and J. Wang, “HRFormer: High-resolution vision transformer for dense predict,” in *NeurIPS*, 2021.

[82] X. Dong, J. Bao, D. Chen, W. Zhang, N. Yu, L. Yuan, D. Chen, and B. Guo, “CSWin transformer: A general vision transformer backbone with cross-shaped windows,” in *CVPR*, 2022.

[83] Y. Lee, J. Kim, J. Willette, and S. J. Hwang, “MPViT: Multi-path vision transformer for dense prediction,” in *CVPR*, 2022.

[84] Y. Li, T. Yao, Y. Pan, and T. Mei, “Contextual transformer networks for visual recognition,” *TPAMI*, 2022.

[85] Y.-H. Wu, Y. Liu, X. Zhan, and M.-M. Cheng, “P2T: Pyramid pooling transformer for scene understanding,” *arXiv preprint arXiv:2106.12011*, 2021.

[86] Z. Li, Y. Liu, B. Li, B. Feng, K. Wu, C. Peng, and W. Hu, “SDTP: Semantic-aware decoupled transformer pyramid for dense image prediction,” *TCSVT*, 2022.

[87] Z. Chen, Y. Duan, W. Wang, J. He, T. Lu, J. Dai, and Y. Qiao, “Vision transformer adapter for dense predictions,” *arXiv preprint arXiv:2205.08534*, 2022.

[88] B. Graham, A. El-Nouby, H. Touvron, P. Stock, A. Joulin, H. Jégou, and M. Douze, “LeViT: a vision transformer in ConvNet’s clothing for faster inference,” in *ICCV*, 2021.

[89] H. Cai, C. Gan, and S. Han, “EfficientViT: Enhanced linear attention for high-resolution low-computation visual recognition,” *arXiv preprint arXiv:2205.14756*, 2022.

[90] Y. Li, G. Yuan, Y. Wen, E. Hu, G. Evangelidis, S. Tulyakov, Y. Wang, and J. Ren, “EfficientFormer: Vision transformers at MobileNet speed,” *arXiv preprint arXiv:2206.07191*, 2022.

[91] K. Wu, J. Zhang, H. Peng, M. Liu, B. Xiao, J. Fu, and L. Yuan, “TinyViT: Fast pretraining distillation for small vision transformers,” in *ECCV*, 2022.

[92] S. Mehta and M. Rastegari, “MobileViT: Light-weight, general-purpose, and mobile-friendly vision transformer,” in *ICLR*, 2022.

[93] Y. Chen, X. Dai, D. Chen, M. Liu, X. Dong, L. Yuan, and Z. Liu, “Mobile-Former: Bridging MobileNet and transformer,” in *CVPR*, 2022.

[94] L. Wang and K.-J. Yoon, “Knowledge distillation and student-teacher learning for visual intelligence: A review and new outlooks,” *TPAMI*, vol. 44, no. 6, pp. 3048–3068, 2022.

[95] Q. Guo, X. Wang, Y. Wu, Z. Yu, D. Liang, X. Hu, and P. Luo, “Online knowledge distillation via collaborative learning,” in *CVPR*, 2020.

[96] H. Bai, H. Mao, and D. Nair, “Dynamically pruning segformer for efficient semantic segmentation,” in *ICASSP*, 2022.

[97] X. Jin, B. Peng, Y. Wu, Y. Liu, J. Liu, D. Liang, J. Yan, and X. Hu, “Knowledge distillation via route constrained optimization,” in *ICCV*, 2019.

[98] Z. Wu, Y. Jiang, C. Cui, Z. Yang, X. Xue, and H. Qi, “Spirit distillation: Precise real-time semantic segmentation of road scenes with insufficient data,” *arXiv preprint arXiv:2103.13733*, 2021.

[99] L. Liu, Q. Huang, S. Lin, H. Xie, B. Wang, X. Chang, and X. Liang, “Exploring inter-channel correlation for diversity-preserved knowledge distillation,” in *ICCV*, 2021.

[100] Y. Zhu and Y. Wang, “Student customized knowledge distillation: Bridging the gap between student and teacher,” in *ICCV*, 2021.

[101] A. Douillard, Y. Chen, A. Dapogny, and M. Cord, “Tackling catastrophic forgetting and background shift in continual semantic segmentation,” *arXiv preprint arXiv:2106.15287*, 2021.

[102] C. Yang, H. Zhou, Z. An, X. Jiang, Y. Xu, and Q. Zhang, “Cross-image relational knowledge distillation for semantic segmentation,” in *CVPR*, 2022.

[103] Z. Zhang, C. Zhou, and Z. Tu, “Distilling inter-class distance for semantic segmentation,” in *IJCAI*, 2022.

[104] Z. Yang, Z. Li, M. Shao, D. Shi, Z. Yuan, and C. Yuan, “Masked generative distillation,” in *ECCV*, 2022.

[105] J. Song, Y. Chen, J. Ye, and M. Song, “Spot-adaptive knowledge distillation,” *TIP*, vol. 31, pp. 3359–3370, 2022.

[106] T. He, C. Shen, Z. Tian, D. Gong, C. Sun, and Y. Yan, “Knowledge adaptation for efficient semantic segmentation,” in *CVPR*, 2019.

[107] Z. Tian, P. Chen, X. Lai, L. Jiang, S. Liu, H. Zhao, B. Yu, M.-C. Yang, and J. Jia, “Adaptive perspective distillation for semantic segmentation,” *TPAMI*, 2022.

[108] S. Lin, H. Xie, B. Wang, K. Yu, X. Chang, X. Liang, and G. Wang, “Knowledge distillation via the target-aware transformer,” in *CVPR*, 2022.

[109] I. Radosavovic, P. Dollár, R. Girshick, G. Gkioxari, and K. He, “Data distillation: Towards omni-supervised learning,” in *CVPR*, 2018.

[110] G. Yang, E. Fini, D. Xu, P. Rota, M. Ding, M. Nabi, X. Alameda-Pineda, and E. Ricci, “Uncertainty-aware contrastive distillation for incremental semantic segmentation,” *TPAMI*, 2022.

[111] X. Jiao, Y. Yin, L. Shang, X. Jiang, X. Chen, L. Li, F. Wang, and Q. Liu, “TinyBERT: Distilling BERT for natural language understanding,” in *EMNLP*, 2020.

[112] C. Dong, G. Wang, H. Xu, J. Peng, X. Ren, and X. Liang, “EfficientBERT: Progressively searching multilayer perceptron via warm-up knowledge distillation,” in *EMNLP*, 2021.

[113] W. Wang, F. Wei, L. Dong, H. Bao, N. Yang, and M. Zhou, “MiniLM: Deep self-attention distillation for task-agnostic compression of pre-trained transformers,” in *NeurIPS*, 2020.

- [114] N. Shazeer, “GLU variants improve transformer,” *arXiv preprint arXiv:2002.05202*, 2020.
- [115] Y. N. Dauphin, A. Fan, M. Auli, and D. Grangier, “Language modeling with gated convolutional networks,” in *ICML*, 2017.
- [116] X. Li, W. Wang, X. Hu, and J. Yang, “Selective kernel networks,” in *CVPR*, 2019.
- [117] J. Hu, L. Shen, and G. Sun, “Squeeze-and-excitation networks,” in *CVPR*, 2018.
- [118] X. Hu, K. Yang, L. Fei, and K. Wang, “ACNet: Attention based network to exploit complementary features for RGBD semantic segmentation,” in *ICIP*, 2019.
- [119] D. P. Kingma and J. Ba, “Adam: A method for stochastic optimization,” in *ICLR*, 2015.
- [120] H. Zhang, K. Dana, J. Shi, Z. Zhang, X. Wang, A. Tyagi, and A. Agrawal, “Context encoding for semantic segmentation,” in *CVPR*, 2018.
- [121] S. Choi, J. T. Kim, and J. Choo, “Cars can’t fly up in the sky: Improving urban-scene segmentation via height-driven attention networks,” in *CVPR*, 2020.
- [122] Y. Yuan, X. Chen, and J. Wang, “Object-contextual representations for semantic segmentation,” in *ECCV*, 2020.
- [123] R. P. Poudel, U. Bonde, S. Liwicki, and C. Zach, “ContextNet: Exploring context and detail for semantic segmentation in real-time,” in *BMVC*, 2018.
- [124] T. Wu, S. Tang, R. Zhang, J. Cao, and Y. Zhang, “CGNet: A light-weight context guided network for semantic segmentation,” *TIP*, vol. 30, pp. 1169–1179, 2021.
- [125] M. Tan and Q. Le, “EfficientNet: Rethinking model scaling for convolutional neural networks,” in *ICML*, 2019.
- [126] J. Xie, B. Shuai, J.-F. Hu, J. Lin, and W.-S. Zheng, “Improving fast segmentation with teacher-student learning,” in *BMVC*, 2018.
- [127] L. Van der Maaten and G. Hinton, “Visualizing data using t-SNE,” *JMLR*, vol. 9, no. 11, 2008.